

OCT 9 1977
OAK RIDGE NATIONAL LABORATORY

Conservation
—
Division of Buildings
and
Community Systems

Performance Evaluation of a Low-First-Cost, Three-Ton, Air-to-Air Heat Pump in the Heating Mode

A. A. Domingorena



OAK RIDGE NATIONAL LABORATORY
OPERATED BY UNION CARBIDE CORPORATION · FOR THE DEPARTMENT OF ENERGY

Printed in the United States of America. Available from
National Technical Information Service
U.S. Department of Commerce
5285 Port Royal Road, Springfield, Virginia 22161
Price: Printed Copy \$6.00; Microfiche \$3.00

This report was prepared as an account of work sponsored by an agency of the United States Government. Neither the United States Government nor any agency thereof, nor any of their employees, contractors, subcontractors, or their employees, makes any warranty, express or implied, nor assumes any legal liability or responsibility for any third party's use or the results of such use of any information, apparatus, product or process disclosed in this report, nor represents that its use by such third party would not infringe privately owned rights.

Contract No. W-7405-eng-26

Energy Division

PERFORMANCE EVALUATION OF A LOW-FIRST-COST,
THREE-TON, AIR-TO-AIR HEAT PUMP
IN THE HEATING MODE

A. A. Domingorena

DEPARTMENT OF ENERGY
Division of Buildings and Community Systems

Date Published: October 1978

OAK RIDGE NATIONAL LABORATORY
Oak Ridge, Tennessee 37830
operated by
UNION CARBIDE CORPORATION
for the
DEPARTMENT OF ENERGY

CONTENTS

LIST OF FIGURES	v
LIST OF TABLES	vii
ABSTRACT	1
1. INTRODUCTION	1
2. SUMMARY AND CONCLUSIONS	2
2.1 Heating Capacity and Coefficient of Performance (COP) under Steady-State (Nonfrosting) Conditions	2
2.2 Fan and Fan-Motor Efficiency	3
2.3 Heat-Exchanger and Capillary-Tube Performance	3
2.4 Heat Losses	4
2.5 Compressor Operation	4
2.6 Performance under Frosting Conditions	5
2.7 Effect of Component Inefficiencies	6
2.8 Effect of Refrigerant Charge	8
3. DESCRIPTION OF TEST UNIT	8
4. DESCRIPTION OF TEST APPARATUS	9
4.1 Test Loops	9
4.2 Instrumentation	10
4.2.1 Temperature	10
4.2.2 Pressure	14
4.2.3 Refrigerant flow rate	14
4.2.4 Airflow rate	14
4.2.5 Electrical power input	14
4.2.6 Humidity	15
4.3 Data Acquisition System	15
5. TEST PROCEDURE	15
5.1 Steady-State Tests	15
5.2 Frosting-Defrosting Tests	17
5.3 Fan Tests	18
5.4 Variable Refrigerant Charge Test	19
6. STEADY-STATE TEST RESULTS	19
6.1 Heating Capacity and COP	20
6.2 Fan Performance	23

6.2.1	Indoor-unit fan	23
6.2.2	Outdoor-unit fan	27
6.2.3	Incentives for improving fan efficiency	27
6.3	Heat-Exchanger and Capillary-Tube Performance	29
6.3.1	Condenser (indoor coil)	30
6.3.2	Evaporator (outdoor coil)	33
6.4	System Heat Losses	33
6.5	Compressor Operation	36
7.	FROSTING-DEFROSTING TEST RESULTS	39
7.1	System Performance under Frosting Conditions	39
7.1.1	Tests at 2.5°C	39
7.1.2	Tests at -3°C	45
7.1.3	Defrost water collection	51
7.2	Compressor Performance during Defrost Period	52
7.3	Average COP for the Frosting-Defrosting Cycle	58
8.	REFRIGERANT CHARGE VARIATION TESTS	60
	ACKNOWLEDGMENTS	66
	REFERENCE	66
	APPENDIX A -- SYSTEM DESCRIPTION	69
A.1	Heat-Pump Manufacturer Ratings and Description of Heat-Pump Components	69
A.2	Schematic and Details of the Outdoor and Indoor Heat Exchangers	70
A.2.1	Outdoor unit	70
A.2.2	Indoor unit	73
	APPENDIX B -- STEADY-STATE (NO-FROST) EXPERIMENTAL DATA	76
	APPENDIX C -- FAN-MOTOR PERFORMANCE CURVES	79
C.1	Centrifugal Fan (Indoor Unit)	79
C.2	Propeller Fan (Outdoor Unit)	80

LIST OF FIGURES

<u>Number</u>	<u>Title</u>	<u>Page</u>
2.1	Effect of component inefficiencies on system efficiency under steady-state, nonfrosting conditions	7
4.1	Experimental apparatus	11
4.2	Schematic diagram of outdoor-unit test loop	12
4.3	Schematic diagram of indoor-unit test loop	13
4.4	Data acquisition system	16
6.1	System performance as a function of outdoor air temperature	21
6.2	Power input as a function of outdoor air temperature	22
6.3	Effect of indoor-fan speed on system performance	24
6.4	Effect of indoor air temperature on system performance	25
6.5	Indoor-fan characteristics	26
6.6	Outdoor-fan characteristics	28
6.7	Temperature profile of indoor coil at return bends	32
7.1	Heating capacity and COP during 90-min frosting period with outdoor air at 2.5°C	40
7.2	Outdoor coil air pressure drop and airflow rate during 90-min frosting period with outdoor air at 2.5°C	41
7.3	Suction and high-side refrigerant pressure during 90-min frosting period with outdoor air at 2.5°C	42
7.4	Compressor and outdoor-fan-power consumption during 90-min frosting period with outdoor air at 2.5°C	43
7.5	Refrigerant mass flow rate during 90-min frosting period with outdoor air at 2.5°C	44
7.6	Heating capacity and COP during 60-min frosting period with outdoor air at -3°C	46
7.7	Outdoor coil air pressure drop and airflow rate during 60-min frosting period with outdoor air at -3°C	47
7.8	Suction and high-side refrigerant pressure during 60-min frosting period with outdoor air at -3°C	48
7.9	Compressor and outdoor-fan power consumption during 60-min frosting period with outdoor air at -3°C	49
7.10	Refrigerant mass flow rate during 60-min frosting period with outdoor air at -3°C	50

<u>Number</u>	<u>Title</u>	<u>Page</u>
7.11	Power consumption and system pressures during defrost period after 30-min frosting with outdoor air at 2.5°C	53
7.12	Power consumption and system pressures during defrost period after 90-min frosting with outdoor air at 2.5°C	54
7.13	Power consumption and system pressures during defrost period after 30-min frosting with outdoor air at -3°C	55
7.14	Power consumption and system pressures during defrost period after 60-min frosting with outdoor air at -3°C	56
8.1	High-side and suction-side pressures as functions of refrigerant charge	61
8.2	Suction gas superheat as a function of refrigerant charge	62
8.3	Refrigerant mass flow rate as a function of refrigerant charge	63
8.4	Heating capacity as a function of refrigerant charge	64
8.5	COP as a function of refrigerant charge	65
A.1	Schematic of outdoor-coil refrigerant circuit in the heating mode	71
A.2	Outdoor-coil construction detail and refrigerant circuit in the heating mode	72
A.3	Indoor unit schematic	74
A.4	Schematic of indoor-coil refrigerant circuit in the heating mode	75
B.1	Schematic of refrigerant circuit, air path, and thermodynamic cycle in the heating mode	78

LIST OF TABLES

<u>Number</u>	<u>Title</u>	<u>Page</u>
3.1	Principal features of test unit	9
5.1	Steady-state test plan	17
5.2	Frosting-defrosting test sequence	18
6.1	Steady-state indoor-coil (condenser) performance	31
6.2	Steady-state outdoor-coil (evaporator) performance	34
6.3	System heat losses	35
6.4	Compressor operating parameters	37
7.1	Frost accumulation as approximated by defrost water drain collection	51
7.2	Average COP over frosting-defrosting cycle	59
B.1	Steady-state test data	77
C.1	Indoor-fan test data	79
C.2	Overall efficiency of the indoor-fan-motor unit as a function of airflow rate	79
C.3	Outdoor-fan test data	80
C.4	Overall efficiency of the outdoor-fan-motor unit as a function of airflow rate	80

PERFORMANCE EVALUATION OF A LOW-FIRST-COST, THREE-TON,
AIR-TO-AIR HEAT PUMP IN THE HEATING MODE

A. A. Domingorena

ABSTRACT

A low-cost, air-to-air, split-system residential heat pump of nominal 3-ton capacity was instrumented and tested in the heating mode under laboratory conditions. This was the first of a planned series of experiments, the objective of which is to assemble a detailed data base of system and component performance for heat pumps. The system was tested under both steady-state and frosting-defrosting conditions.

From the steady-state tests, the heating capacity and coefficient of performance were determined, and evaluations of fan performance, heat-exchanger and capillary-tube performance, compressor performance, and system heat losses were made. The frosting-defrosting tests provided information for evaluating both system and component performance under dynamic conditions.

Tests were also conducted to determine the effect of the amount of refrigerant charge on system performance.

1. INTRODUCTION

This report describes the procedures and results of experiments being conducted as a part of a heat-pump research program by the Oak Ridge National Laboratory for the Department of Energy, Office of Conservation and Solar Applications, Division of Buildings and Community Systems. The overall objective of the research program is to identify and promote cost-effective modifications in heat-pump design that can substantially reduce energy consumption in residential and commercial buildings. This objective is being approached in a combined experimental and theoretical study. A data base on heat-pump system and component performance is being obtained experimentally, and a computer model is being formulated to evaluate analytically various candidate improvements. In order to provide the level of detail required for these analyses, the procedures used in the experimental tests will be much more extensive

than those required for rating heat pumps for consumer comparative purposes. The emphasis will be on gathering information for design studies rather than providing consumer information.

The specific objectives of the experiments described herein are:

1. to determine the base-case performance of a low-first-cost heat pump and the characteristics of some of its components under steady-state nonfrosting conditions and frosting-defrosting conditions,
2. to measure experimentally the degradation of heat-pump performance due to frost accumulation on the outdoor coil.

It was decided at the outset of the study that one of the heat-pump units to be tested should be a low-cost system that might be selected by a speculative home builder. It is planned to test, at a later time, other units that have different features and higher efficiency ratings.

Tests were conducted on a nominal 3-ton, air-to-air, split-system heat pump consisting of an indoor and an outdoor unit separated by 7.6 m (25 ft) of liquid-line and vapor-line refrigerant tubing. The system was instrumented so that the performance of both individual components and the total system could be evaluated. The test facility consisted of two "bootstrap" air duct loops which are described subsequently in this report.

2. SUMMARY AND CONCLUSIONS

2.1 Heating Capacity and Coefficient of Performance (COP) under Steady-State (Nonfrosting) Conditions

The observed capacity and efficiency of the system under steady-state nonfrosting conditions were found to compare closely with rated values. The observed and rated performance parameters for operation at 8°C (47°F) outdoor air temperature and 21°C (70°F) indoor air temperature are as follows:

Observed heating capacity, refrigerant method, kW	10.90
Observed heating capacity, air method, kW	11.10

Rated heating capacity, kW	11.40
COP, refrigerant method	2.08
COP, air method	2.13
Rated COP	2.20
Observed power input, kW	5.21
Rated power input, kW	5.10

The heating capacity and COP were measured by two methods, air-side heat balance and refrigerant-side heat balance, which yielded reasonably consistent results. Reducing the indoor-fan speed from 850 rpm to 650 rpm produced no observable effect on the unit's performance, although a 3% drop in capacity and COP was observed when the fan speed was further reduced to 460 rpm. Decreasing the indoor air temperature from 21°C (70°F) to 18°C (65°F) had no observable effect on the performance of the unit, contrary to expectations, but increasing the indoor air temperature to 27°C (80°F) caused an expected small drop in capacity and COP.

2.2 Fan and Fan-Motor Efficiency

The combined efficiency (power spent in moving air divided by electrical input) of the indoor fan and fan-motor at the nominal airflow rate of 2000 m³/hr (1200 ft³/min) is 0.17, while peak efficiency of the fan and motor is 0.22, obtained at about 1600 m³/hr (940 ft³/min). For the outdoor fan and motor, the combined efficiency at the nominal airflow rate of 4000 m³/hr (2350 ft³/min) is 0.11, while peak efficiency of 0.13 is obtained at 3100 m³/hr (1800 ft³/min). Accordingly, it is concluded that the fans are not operating in their best-efficiency operating regime as installed in the test apparatus. Some opportunity for improvement in combined fan and fan-motor efficiency is apparent. An analysis of the quick payback expected from such an improvement is given later in this report.

2.3 Heat-Exchanger and Capillary-Tube Performance

The performance of the heat-exchanger components is related to the flow characteristics of the capillary-tube control device. Both the indoor and outdoor coils operate with a close approach of refrigerant exit temperature to entering air temperature: 3–5 C° (5–9 F°) in the indoor coil and 2–6 C° (4–11 F°) in the outdoor coil. However, a high indoor-coil condensing temperature [up to 36 C° (65 F°) above indoor air temperature] is maintained by the restriction of the capillary-tube control. In the outdoor (evaporating) coil, the capillary-tube control results in zero exit superheat under cold [below 0°C (32°F)] outdoor conditions, and superheat ranging up to 16°C (28°F) in warmer ambients. The indoor coil appears to run typically one-half full of liquid refrigerant in the heating mode, as evidenced by measurement of return-bend temperatures.

2.4 Heat Losses

It is apparent that about 1.6 kW (5500 Btu/hr) are being rejected as heat from the bare compressor shell — approximately one-third of compressor power input. While this helps cool the compressor, it results in a system efficiency loss. In the discharge line, 0.15 to 0.65 kW (500 to 2200 Btu/hr) are being lost; presumably, most of this occurs at or in the reversing valve.

2.5 Compressor Operation

The overall compressor efficiency, defined as the ratio of ideal isentropic work (based on shell inlet and outlet conditions) to actual electrical energy input, ranged from 0.40 to 0.44. (It was not possible to compute compressor efficiency for operating conditions under which compressor-suction vapor was in the wet, saturated condition.) This efficiency level is judged to be low compared with what is achievable within the present state of the art.

2.6 Performance under Frosting Conditions

Of the two outdoor conditions under which frosting performance was evaluated (-3°C and 2.5°C , both with 90–100% relative humidity), the lower temperature proved to be the more severe in terms of rate of frost accumulation on the outdoor coil. The following tabulation gives a performance summary (percent change) for the system after one-half hour of frosting operation:

	<u>-3°C ($26\text{--}27^{\circ}\text{F}$)</u>	<u>2.5°C ($36\text{--}37^{\circ}\text{F}$)</u>
Outdoor-coil airflow	-47	-19
Outdoor-coil air pressure drop	+240	+238
Heating capacity	-14	-7
COP	-10	-3
Outdoor-fan power	+4	+4

The system was capable of operating for 90 min at 2.5°C and 60 min at -3°C , at which time outdoor-coil airflow was severely restricted and system pressures were decreasing rapidly.

Defrost water collection ranged from 1.0 to 1.3 liters after one-half-hour frosting periods. After a 90-min frosting period at 2.5°C , 2.8 liters of water were collected.

Records of transient system pressures during the defrost cycle show that, 1 min after initiation of the cycle, system pressures are extremely low — the result of condensation and accumulation of refrigerant in the cold outside coil. Another minute of operation is required before nominal pressures begin to be restored and heat is delivered to the outside coil at a significant rate.

The average COP during frosting-defrosting conditions takes into account the power input required during defrost. If the system is also penalized by the supplementary electric resistance heat required to maintain full heating capacity, the average COP is further reduced. Computed average COPs over a 30-min frosting cycle are as follows:

Temperature (°C)	Coefficient of performance		
	<u>Nonfrosting</u>	<u>Without supplementary resistance heat</u>	<u>With supplementary resistance heat</u>
2.5	2.05	1.73	1.60
-3.0	2.00	1.56	1.42

2.7 Effect of Component Inefficiencies

Figure 2.1 shows the manner in which the observed component inefficiencies affect the system efficiency, or COP, for the nonfrosting conditions of 21°C (70°F) indoor and 8°C (47°F) outdoor air temperatures. An ideal vapor-compression cycle using R-22 as the working fluid and operating between the temperature limits of 21 and 8°C (70 and 47°F) has a COP of 21.45. Of course, a real system cannot operate without a temperature difference across the heat exchangers. For an ideal R-22 system using the observed heat-exchanger temperatures,

53°C (127°F) condensing,
 -3°C (26°F) evaporating,
 27 C° (48 F°) subcooling,
 11 C° (19 F°) superheat,

the computed COP is 5.41. Thus a 75% loss in efficiency from the ideal, reversible cycle results from the temperature differences across the heat exchangers. A compressor efficiency of 0.42 reduces the COP to 2.85, an additional 47% loss. Heat loss from the compressor shell as measured in these tests reduces the computed COP 14% to 2.45. The ideal fan power would reduce the COP 3% to 2.38; and the observed fan and fan-motor inefficiencies further reduce the computed COP an additional 12%, to 2.09 -- which is about equal to the observed COP.

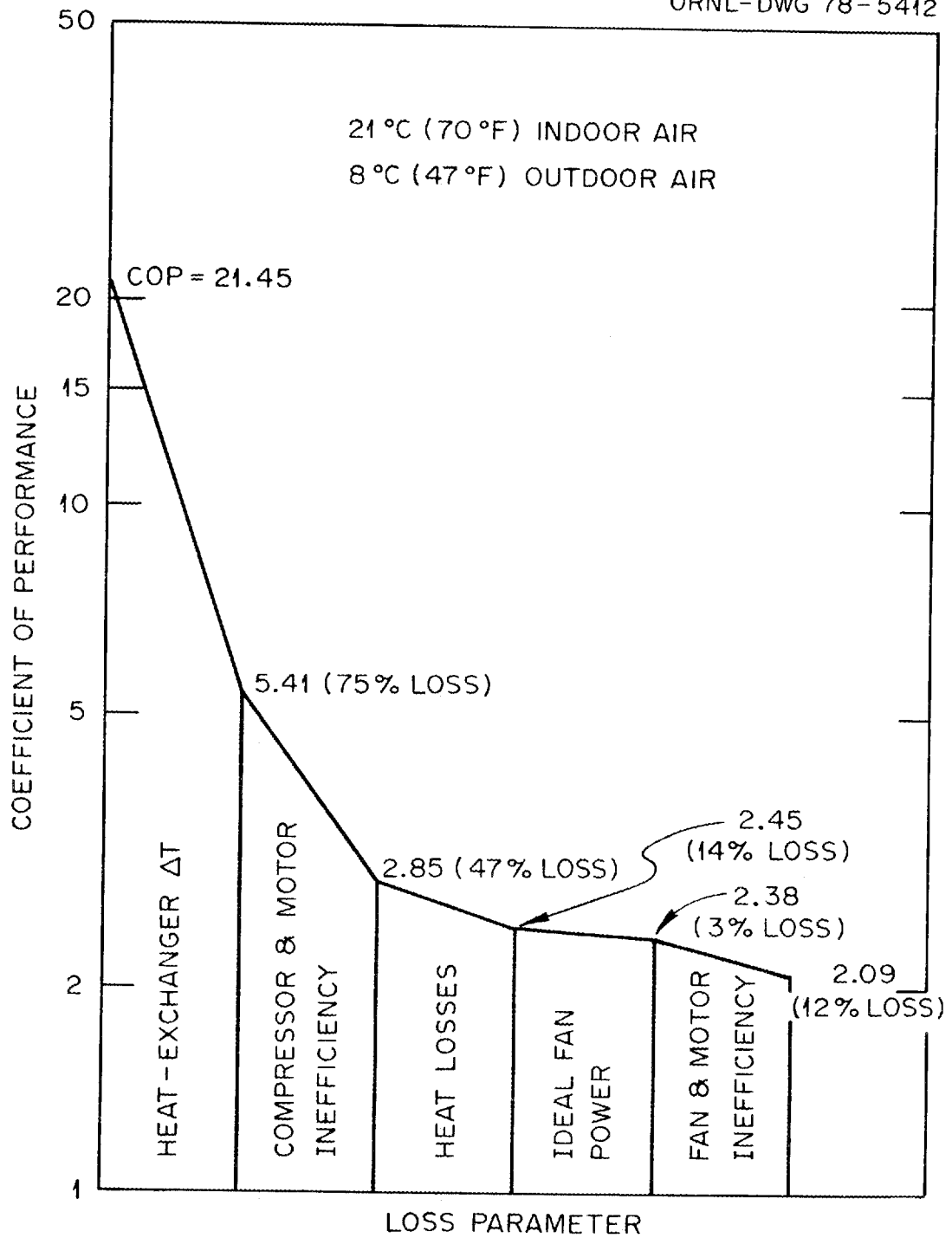


Fig. 2.1. Effect of component inefficiencies on system efficiency under steady-state, nonfrosting conditions.

2.8 Effect of Refrigerant Charge

The experimental results indicate that the performance of the system is highly sensitive to refrigerant undercharge. There is an almost linear reduction in the heating capacity and COP as the refrigerant charge decreases from the nominal charge of 3.4 kg (7 lb, 9 oz) to about 1.84 kg (4 lb, 1 oz). On the other hand, overcharging refrigerant to about 3.85 kg (8 lb, 8 oz) results in a small variation of the heating capacity and COP.

3. DESCRIPTION OF TEST UNIT

The heat-pump unit evaluated in this study is a commercially available air-to-air split system with a nominal 3-ton capacity. The salient features of the test unit are presented in Table 3.1; more detailed information on the unit is presented in Appendix A.

The defrost control operates on a time-and-temperature principle. A thermostat located at the bottom of the outdoor coil causes a timer motor to start when the temperature of the outdoor-coil tube drops to 0°C (32°F). After an accumulated period of time at 0°C (32°F) or below, the timer energizes the defrost relays, which in turn position the reversing valve in the cooling mode (defrost period) and stop the outdoor fan. The time at or below 0°C (32°F) that may be accumulated before the defrost cycle is initiated depends on the cam installed in the timer; stock cams are available for either 30 or 90 min.

The unit remains in the defrost period (cooling mode) until the temperature of the outdoor coil reaches 14°C (57°F). At this temperature the coil is essentially free of frost, and the defrost thermostat opens to stop the timer, returning the reversing valve to the heating mode and starting the outdoor fan. The timer will not run again until the outdoor-coil temperature drops to 0°C (32°F).

Table 3.1. Principal features of test unit

Refrigerant	R-22
Compressor	Hermetic Two-piston, reciprocating Two-pole motor $74.1 \times 10^{-6} \text{ m}^3$ (4.52 in. ³) displacement
Outdoor coil	Aluminum fin, copper tube with return bends, three rows deep 0.482 m ² (5.19 ft ²) face area Three-blade, 0.51-m-diam (20-in.) propeller fan 4000 m ³ /hr (2350 cfm) nominal airflow
Indoor coil	Aluminum fin, copper tube with return bends, three rows deep 0.269 m ² (2.90 ft ²) face area 0.23-m-diam (9-in.), 0.2-m-long (8-in.) squirrel-cage fan rotor 2000 m ³ /hr (1200 cfm) nominal airflow
Controls	Capillary tubes for both heating and cooling Time-temperature defrost control Four-way reversing valve
Accumulator	None
Rated capacity	10.55 kW (36,000 Btu/hr) cooling at 35°C (95°F) 11.40 kW (39,000 Btu/hr) heating at 8°C (47°F) 6.50 kW (22,000 Btu/hr) heating at -8°C (17°F)
Rated COP	2.2 at 8°C (47°F) 1.4 at -8°C (17°F)

4. DESCRIPTION OF TEST APPARATUS

4.1 Test Loops

"Bootstrap" air loops were used to control the conditions of the air approaching the indoor and outdoor heat-pump units. In a bootstrap loop, most of the air discharged from the fan-coil unit is recirculated back to the inlet, with bleed air and/or supplemental heat used to control the temperature of the air within the loop. In the indoor-unit loop, cool room air can be injected in the winter to compensate for the heat rejected by the coil, to maintain a desired temperature level. In the summer, this approach is not feasible, and air from a separate

heat-pump system operating in the cooling mode was injected to maintain the desired loop air temperature.

The temperature of the inlet air to the outdoor-unit loop, which is reduced by the cold outdoor coil (in the heating mode), is regulated either by bleeding in room air or by adding electric resistance heat. Humidity can be controlled by injecting steam into the loop.

In this study the steady-state tests (nonfrosting) were conducted in winter, and the ambient laboratory air was dry enough to preclude frosting. The frosting-defrosting tests were conducted in summer, and laboratory air bled into the outdoor-unit test loop was sufficiently humid to provide essentially 100% relative humidity in the loop. This was a desirable condition because it represented a "most severe" operating environment.

Bootstrap loops have a shortcoming in conducting cycling and defrosting tests: control of the air temperature in the outdoor-unit loop is lost during the "off" or defrosting period. Thus, some time after startup is required to reestablish the desired test conditions. In our tests, the time required to reestablish the desired outdoor air temperature after defrosting was 6-10 min. However, the subsequent frosting period was assumed to commence only after the coil temperature dropped below 0°C (32°F).

Figure 4.1 is a photograph of the test loops used in this study, and Figs. 4.2 and 4.3 are schematics of the outdoor and indoor loops respectively. The loops are operated without a supplementary fan; this is possible because large flow areas and corresponding low air velocities are maintained, and a low-pressure-drop airflow measurement scheme is employed.

4.2 Instrumentation

4.2.1 Temperature

All temperatures were measured with Chromel-Alumel thermocouples except for those on the compressor, which were copper-constantan. On refrigerant lines, thermocouples were first taped to the line, then

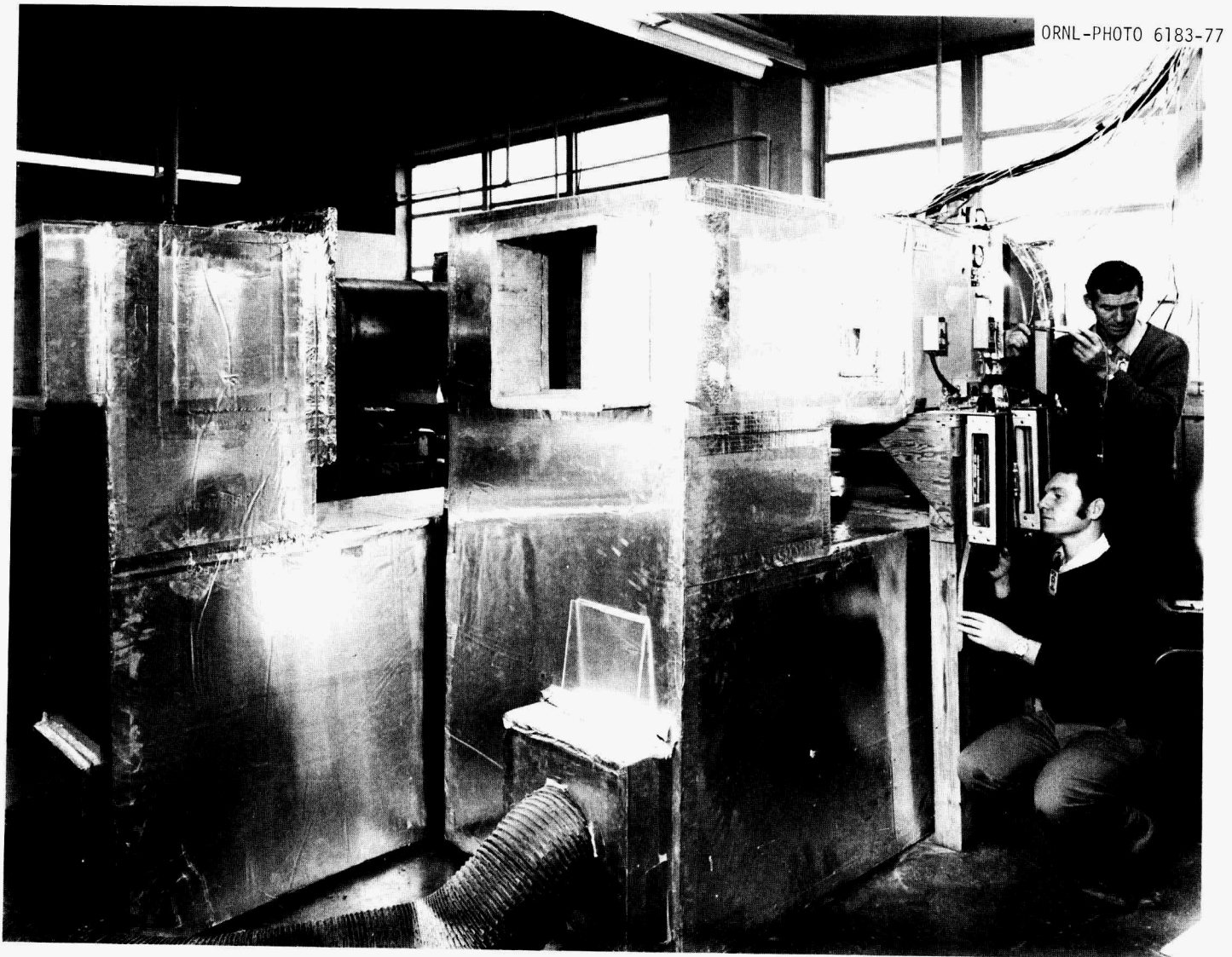


Fig. 4.1. Experimental apparatus.

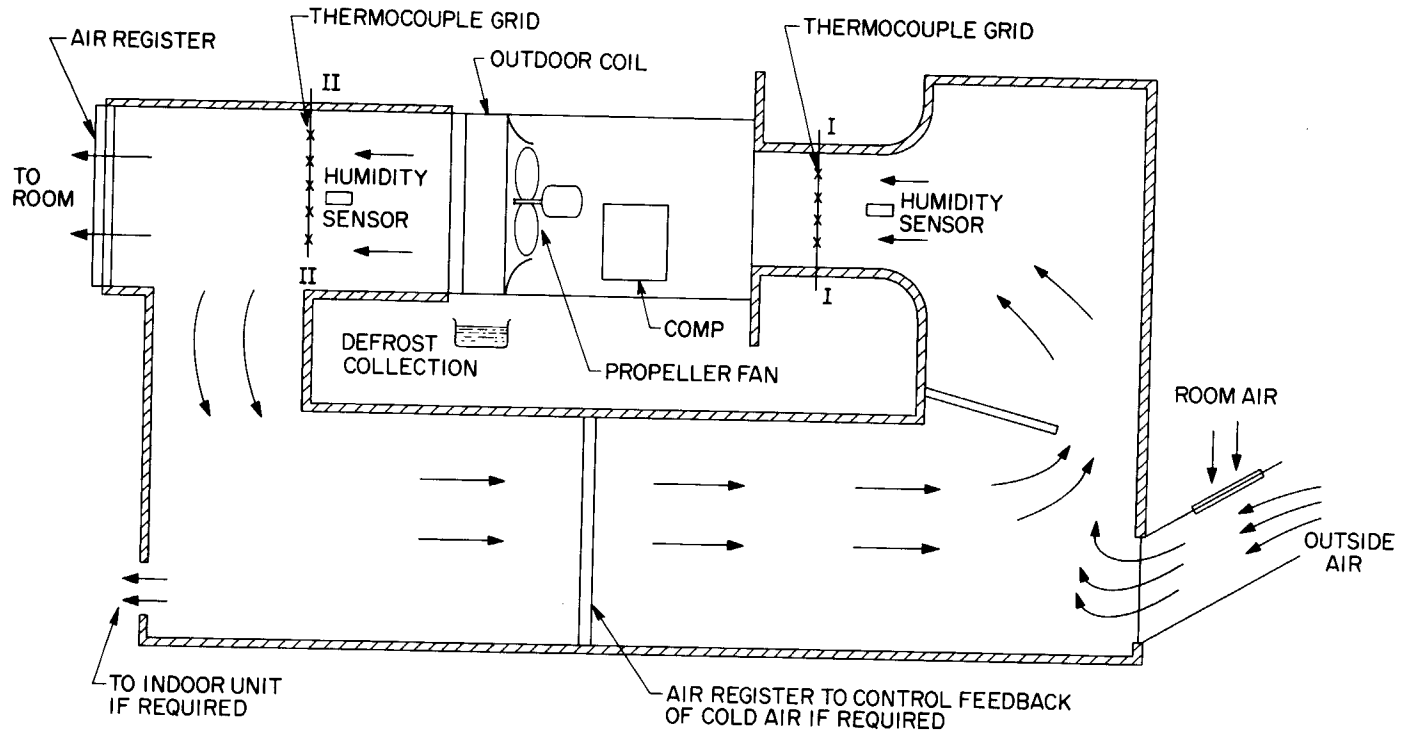


Fig. 4.2. Schematic diagram of outdoor-unit test loop.

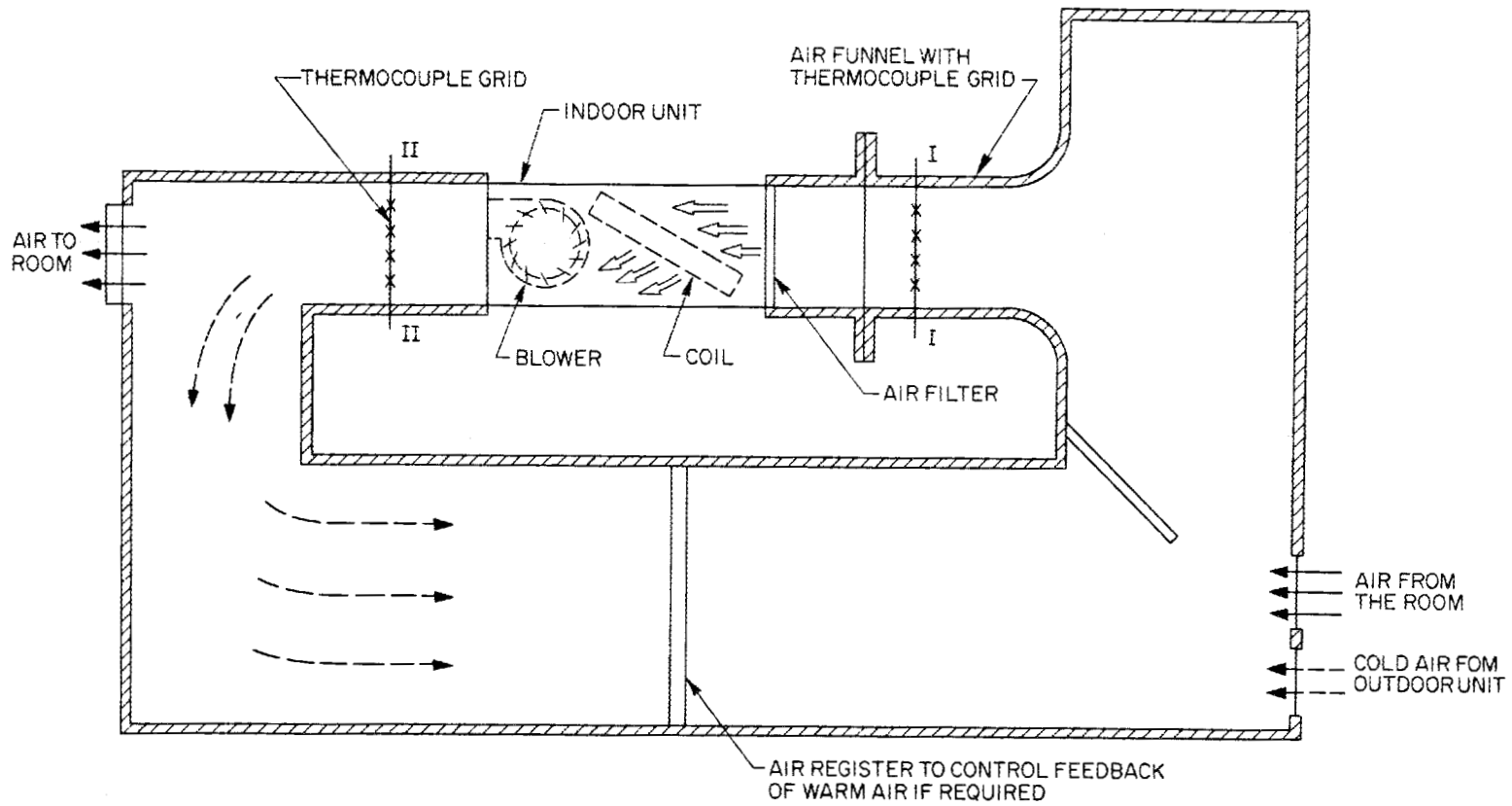


Fig. 4.3. Schematic diagram of indoor-unit test loop.

secured with a hose clamp and covered with foamed-elastomer insulation. Air temperatures were measured by means of thermocouple grids at appropriate locations.

4.2.2 Pressure

Steady-state refrigerant pressures were measured using bourdon-type gages. The low-side pressure gage, with 1-psi divisions, was located at the compressor-shell inlet, and the high-side gage, with 5-psi divisions, was located at the heating-mode capillary-tube inlet. For frosting tests, strain-gage-type dynamic pressure transducers were installed at the same test points.

4.2.3 Refrigerant flow rate

Two rotameters were used to determine refrigerant flow rate. The rotameters were used with a system of check valves so that one was operative in the heating mode and the other was operative in the cooling mode.

4.2.4 Airflow rate

Airflow rate in the test loops was measured by means of velocity traverses, using a hot-wire anemometer. Traverses were made at the air funnels installed in the test loops for this purpose. As previously mentioned, with this low-pressure-loss airflow measuring scheme, it was not necessary to incorporate an auxiliary blower in the loops.

4.2.5 Electrical power input

Power to the compressor and each of the two fans was measured separately. In addition, the system controls were modified so that each component could be switched manually and the defrost cycle could be started and stopped manually. Power input was measured using both watt-hour meters and thermal-watt converters, which produce a dc signal proportional to the instantaneous rate of power consumption.

4.2.6 Humidity

The humidity of the air in the outdoor-unit loop was monitored by means of Aminco type H-3 narrow-range hygrosensors whose operation is based on the ability of a hygroscopic film to change its electrical resistance with changes in the humidity of the air. The humidity sensor for the incoming air was placed inside the air funnel upstream of the outdoor unit, and for the air leaving the coil, it was placed at the thermocouple grid which senses the average dry-bulb temperature of the outdoor air leaving the unit.

4.3 Data Acquisition System

A data acquisition system that automatically records most data parameters was assembled and installed. Refrigerant flow rate and air-flow rate were the only data recorded manually.

The data acquisition system consisted principally of an analog-to-digital converter, a scanner, and a Digital Equipment Corporation PDP8/e minicomputer. The data-output display format and frequency were controlled by the minicomputer. Calibration data entered into the computer were used to convert input signals to the desired units for temperature, pressure, power input, and humidity. The computer was also programmed to print out COP, with refrigerant flow rate entered via the Teletype keyboard.

For most testing, a recording interval of 40 sec was used. Another format was developed for the defrost cycle in which the required parameters were printed out every 10 sec. A photograph of the data acquisition system is shown in Fig. 4.4.

5. TEST PROCEDURE

5.1 Steady-State Tests

For steady-state performance tests, it was planned that the effects of outdoor air temperature, indoor air temperature, and indoor airflow



Fig. 4.4. Data acquisition system.

rate would be investigated. To accomplish this, the test plan shown in Table 5.1 was formulated and followed.

Table 5.1. Steady-state test plan

Outdoor air temperature [°C (°F)]	Indoor air temperature [°C (°F)]	Indoor blower speed (rpm)
-12 (10)	21 (70)	High (850)
- 7 (20)	21 (70)	High (850)
- 1 (30)	21 (70)	High (850)
4 (40)	21 (70)	High (850)
10 (50)	21 (70)	High (850)
16 (60)	21 (70)	High (850)
- 1 (30)	21 (70)	Medium (650)
4 (40)	21 (70)	Medium (650)
10 (50)	21 (70)	Medium (650)
- 1 (30)	21 (70)	Low (460)
4 (40)	21 (70)	Low (460)
10 (50)	21 (70)	Low (460)
- 1 (30)	18 (65)	High (850)
4 (40)	18 (65)	High (850)
10 (50)	18 (65)	High (850)
- 1 (30)	27 (80)	High (850)
4 (40)	27 (80)	High (850)
10 (50)	27 (80)	High (850)

Steady-state tests were conducted by operating the units until stable temperatures were achieved, and then taking data. For steady-state measurements, it was desired that the outdoor unit would be operating in an essentially unfrosted condition, and this was apparently achieved, since no frost was observed.

5.2 Frosting-Defrosting Tests

The sequence of frosting tests is shown in Table 5.2. Tests were conducted at nominal outdoor air temperatures of 3°C (37°F) and -3°C

Table 5.2. Frosting-defrosting test sequence

Outdoor air temperature [°C (°F)]	Relative humidity (%)	Test duration
2.5 (36-37)	90-100	30-min consecutive frosting-defrosting cycles, 3 cycles
2.5 (36-37)	90-100	90-min frosting period, 2 tests
-3 (26-27)	90-100	30-min consecutive frosting-defrosting cycles, 3 cycles
-3 (26-27)	90-100	60-min frosting period

(27°F). Tests were not conducted at 8°C (47°F) because little, if any, frost would be expected at this temperature; -8°C (17°F) was not run because the outdoor test loop would not maintain a temperature that low in the summertime testing environment. The latter temperature is not a severe frosting condition because the specific humidity of air is low in this temperature range.

All tests were conducted at essentially 100% outdoor air relative humidity. It was judged that this "most severe" operating condition (excluding fog or freezing rain) was the most pertinent to investigate.

Because the manufacturer's standard defrost control resulted in a defrost cycle every 30 min of accumulated operation with the outside coil at or below 0°C (32°F), defrost cycles at this frequency were investigated. In addition, longer frosting periods were investigated so that the effect of longer cycle periods on system and component performance could be investigated.

5.3 Fan Tests

Separate tests were conducted to determine the fan-motor efficiencies of both indoor and outdoor units. For these tests, the fans were operated in place, but with the compressor inoperative.

5.4 Variable Refrigerant Charge Test

The influence of the refrigerant charge on the performance of the system in the heating mode was evaluated by varying the charge above and below the value specified by the manufacturer. The evaluation was done while maintaining an outdoor air temperature of 10°C (50°F) dry bulb and a 21°C (70°F) indoor air dry bulb temperature into the indoor unit. The tests were run twice.

The effect of refrigerant charge was first observed starting with the nominal 3.43 kg (7 lb, 9 oz) of refrigerant and undercharging the unit. The undercharge test was stopped when bubbles of refrigerant were observed at about 1.84 kg (4 lb, 1 oz) of refrigerant charge. The refrigerant charge remaining was then evacuated and a vacuum of 740 mm Hg (29 in.) imposed on the refrigerant system for about 12 hr. The system was then charged with 3.43 kg (7 lb, 9 oz) of refrigerant, and the heating capacity was checked. The overcharge tests were then conducted with successively larger amounts of charge until the high pressure switch turned the system off at a high-side pressure of 2450 kPa (355 psia).

6. STEADY-STATE TEST RESULTS

The heating capacity and COP of heat-pump systems as functions of ambient temperature are well documented in manufacturers' literature. Determination of these characteristics of the system was not a primary objective of the experimental program, but such information does provide a check on system performance and is presented here for reference. Obtaining component performance data was considered a more important objective, and discussions of fan, heat-exchanger, and compressor performance follow, in addition to a discussion of system heat losses. Since this is the first test series in our experimental work plan, performance data are, in general, not analyzed on a comparative basis. Steady-state test data are presented in Appendix B.

6.1 Heating Capacity and COP

The heating capacity of a heat pump is defined as the sum of the heat rejected by the indoor coil and the energy input of the indoor fan. The COP is defined as the ratio of heating capacity to total power input, which includes the power to both indoor and outdoor fans and the compressor.

The heating capacity and COP of the system as functions of outdoor air temperature are shown in Fig. 6.1. Data are shown for two methods of determining capacity: one based on the temperature rise of the indoor air, and the other based on the enthalpy change of the refrigerant plus the power to the indoor fan motor. The dashed curves are second-order curve fits to the air-method data, and the solid curves are for the refrigerant method. Heating capacity and COP computed by the air method averages about 3% higher than the same parameters computed by the refrigerant method. The data are more scattered for the air method: standard error in heating capacity is ± 0.37 kW, air method, vs ± 0.16 kW, refrigerant method; standard error in COP is ± 0.08 , air method, vs ± 0.03 , refrigerant method.

Also shown in Fig. 6.1 are the published Air Conditioning and Refrigeration Institute (ARI) rating points for the test unit. Air-method data are about 2% below the ARI rating at 8°C (47°F), while the refrigerant-method results lie about 4% below the ARI point. At the lower rating point [-8°C (17°F)], the observed capacity by either method is slightly greater than the rated capacity. This is to be expected, since the rating procedure at this temperature involves defrosting, while the steady-state tests did not.

Figure 6.2 presents power input data for the system, and it is seen that the experimental data are only about 2% above the ARI rating points.

Figure 6.1 shows the decrease in heating capacity and COP with reduced outdoor air temperature, a relationship that is characteristic of vapor-compression heat-pump systems. The reduced heating capacity is the result of the decrease in suction-gas density and the attendant reduction in refrigerant mass flow rate that occur with colder outdoor-coil temperatures. The decrease in COP is largely due to the increase in

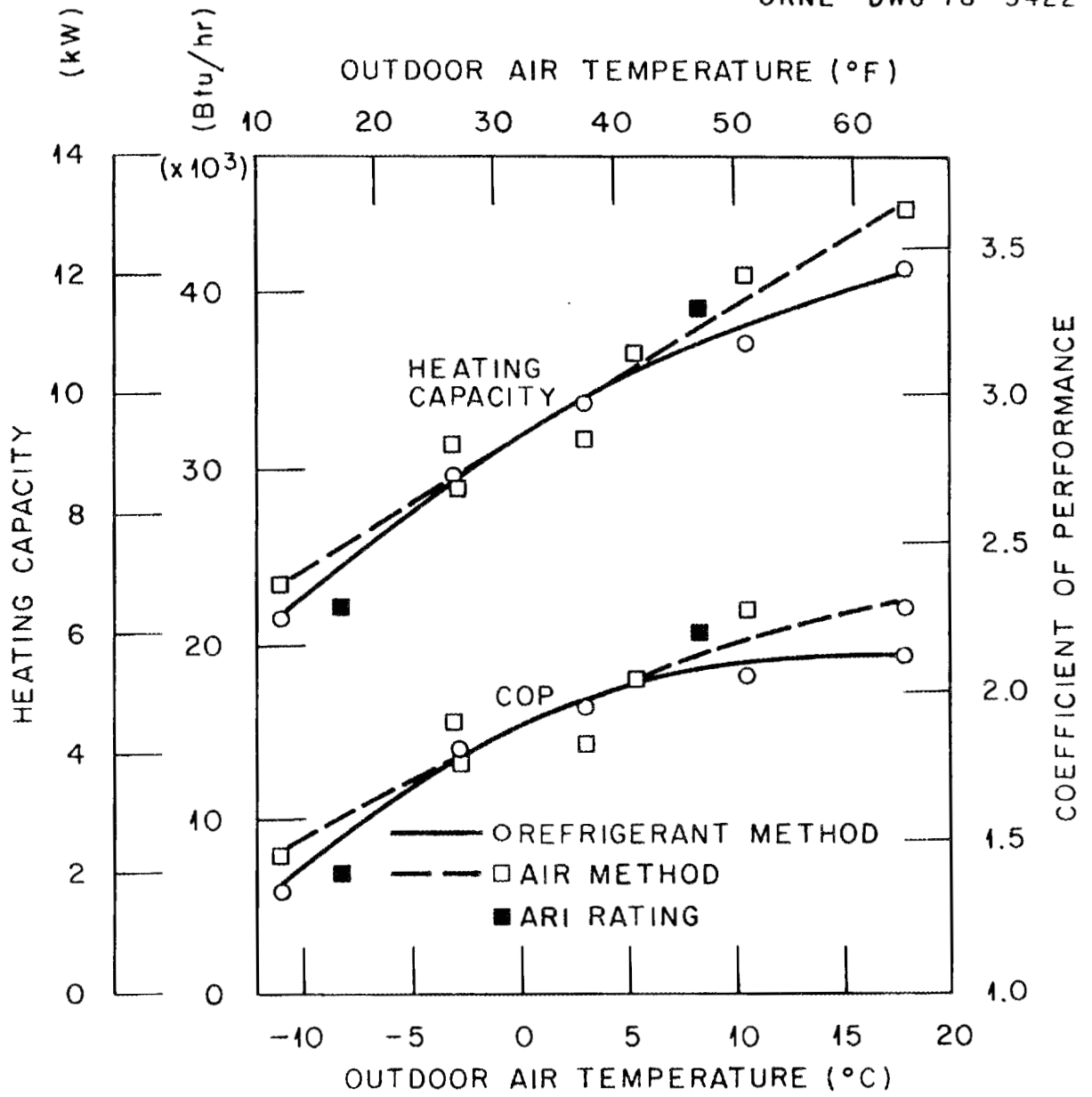


Fig. 6.1. System performance as a function of outdoor air temperature.

ORNL-DWG 78-5421R

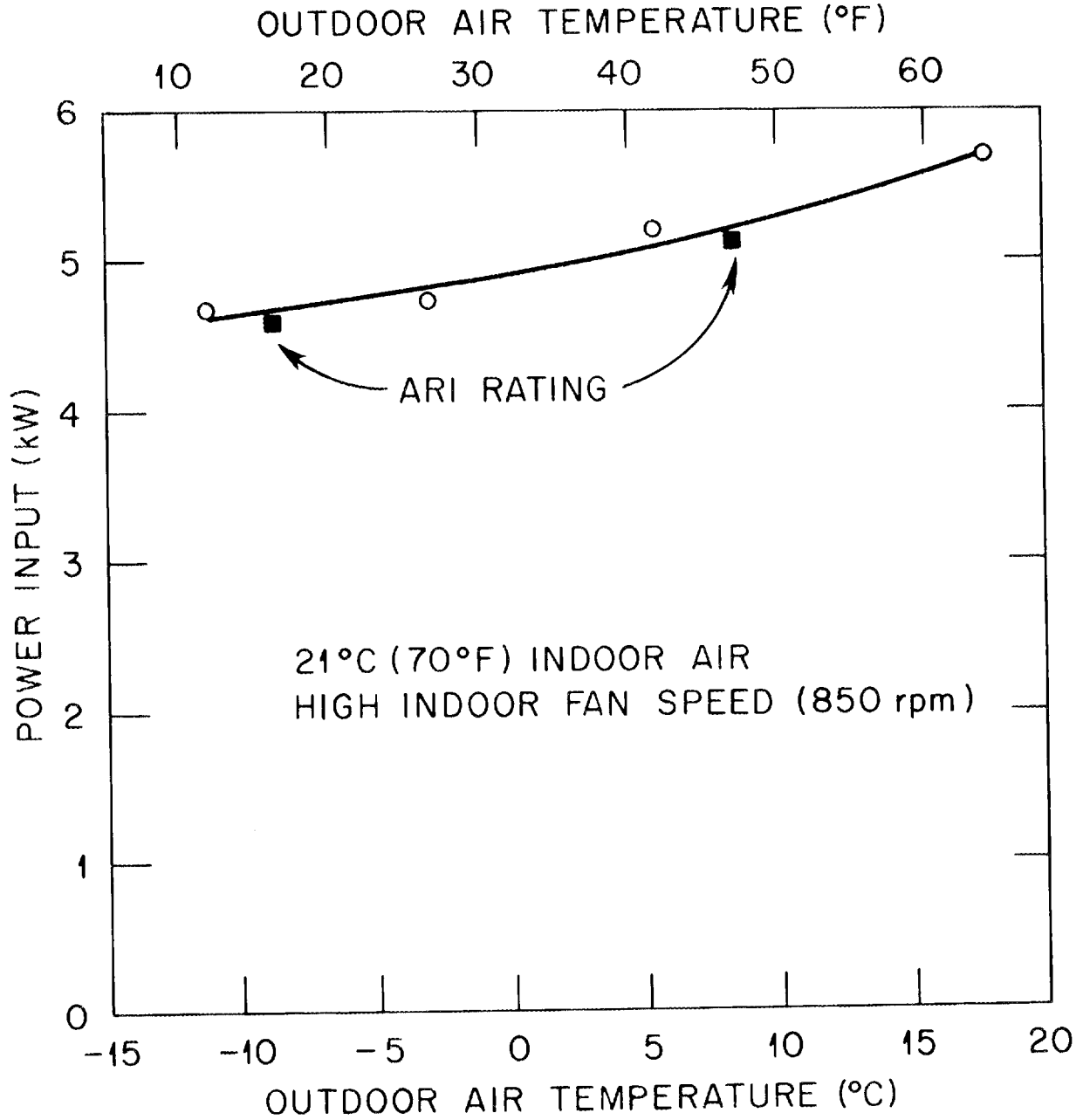


Fig. 6.2. Power input as a function of outdoor air temperature.

compressor pressure ratio, which increases the energy that must be put into the system per unit of refrigerant mass flow.

Figure 6.3 displays the heating capacity as a function of the outdoor air temperature for three indoor-fan speeds: 850, 650, and 460 rpm with the indoor air temperature maintained at about 21°C (70°F). The data show the negligible difference between the heating capacity at 850 and 650 rpm. A decline of about 3% in the heating capacity at 460 rpm is apparent.

Figure 6.3 also shows the effect of indoor-fan speed on COP. There is, again, a negligible difference between the runs at 850 and 650 rpm. At 460 rpm, however, a 4% degradation in the COP can be observed.

A series of runs was conducted to evaluate the effect of indoor air temperature on heating capacity and COP over a range of outdoor air temperatures, maintaining the indoor-fan speed at 850 rpm. Indoor air temperatures of 18, 21, and 27°C (65, 70, and 80°F) were used in these tests. Figure 6.4 shows a trend toward reduced heating capacity and COP with increased indoor air temperature, as would be expected. However, the scatter in the data for the higher indoor air temperatures precludes a meaningful quantitative comparison.

6.2 Fan Performance

6.2.1 Indoor-unit fan

The indoor-unit fan is driven by a 3-speed motor; the speeds are listed by the system manufacturer as 1050, 950, and 850 rpm. Actual fan speeds observed in the laboratory were 850, 650, and 460 rpm.

The results of the indoor-fan test are presented in Fig. 6.5. The efficiency shown is defined as air power delivered divided by electrical power input to the fan motor. Thus, it is a combined fan and motor efficiency and would be equal to the product of the motor efficiency and the fan efficiency, if they were known separately. In the case of the indoor fan, the efficiency is estimated to peak at a value of about 0.22 at a flow rate somewhat below 1170 m³/hr (1000 cfm) and drops rapidly as the flow rate is increased. (All the test points were taken at an airflow rate greater than that at which maximum efficiency is obtained.)

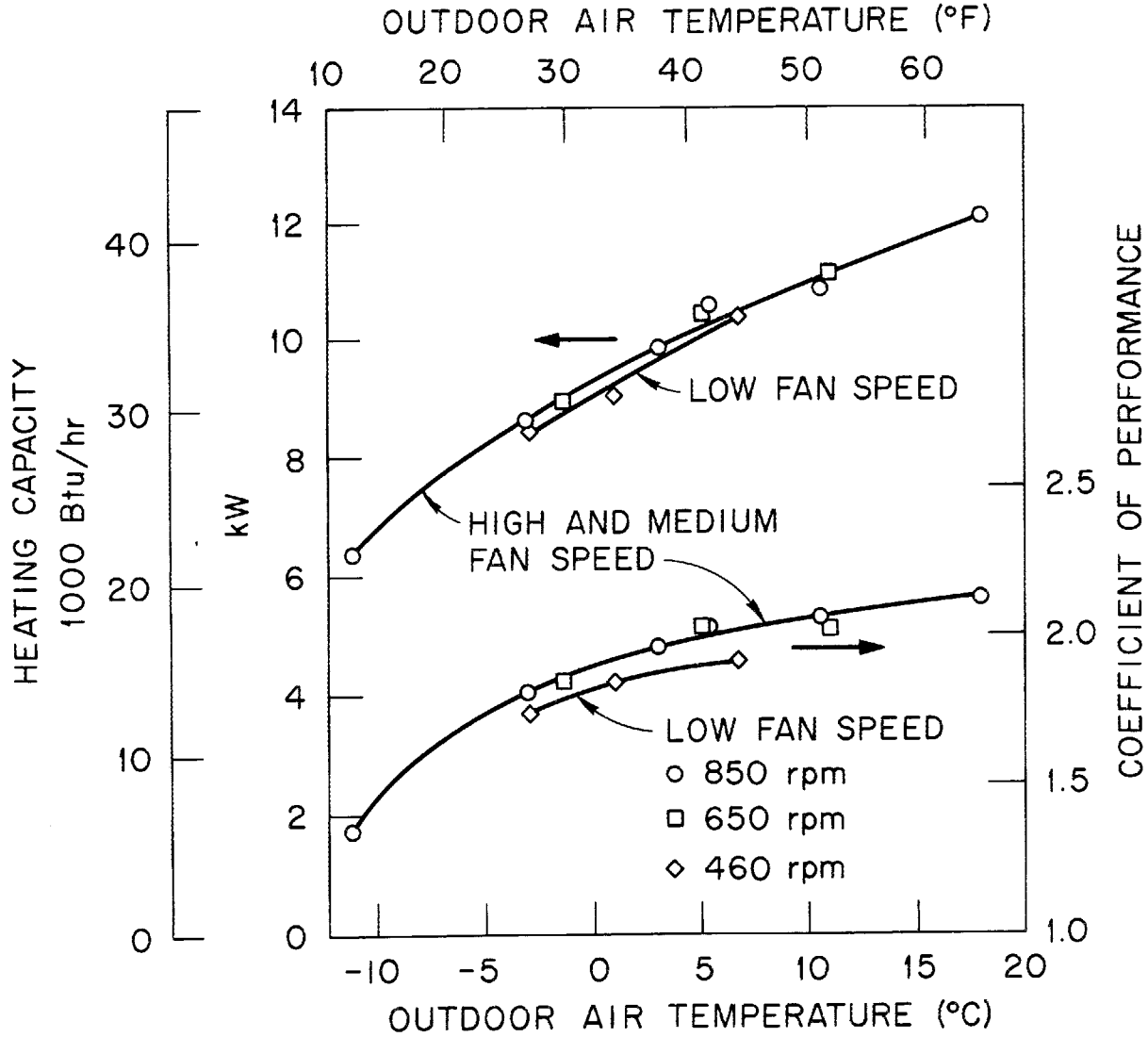


Fig. 6.3. Effect of indoor-fan speed on system performance.

ORNL-DWG 78-6403

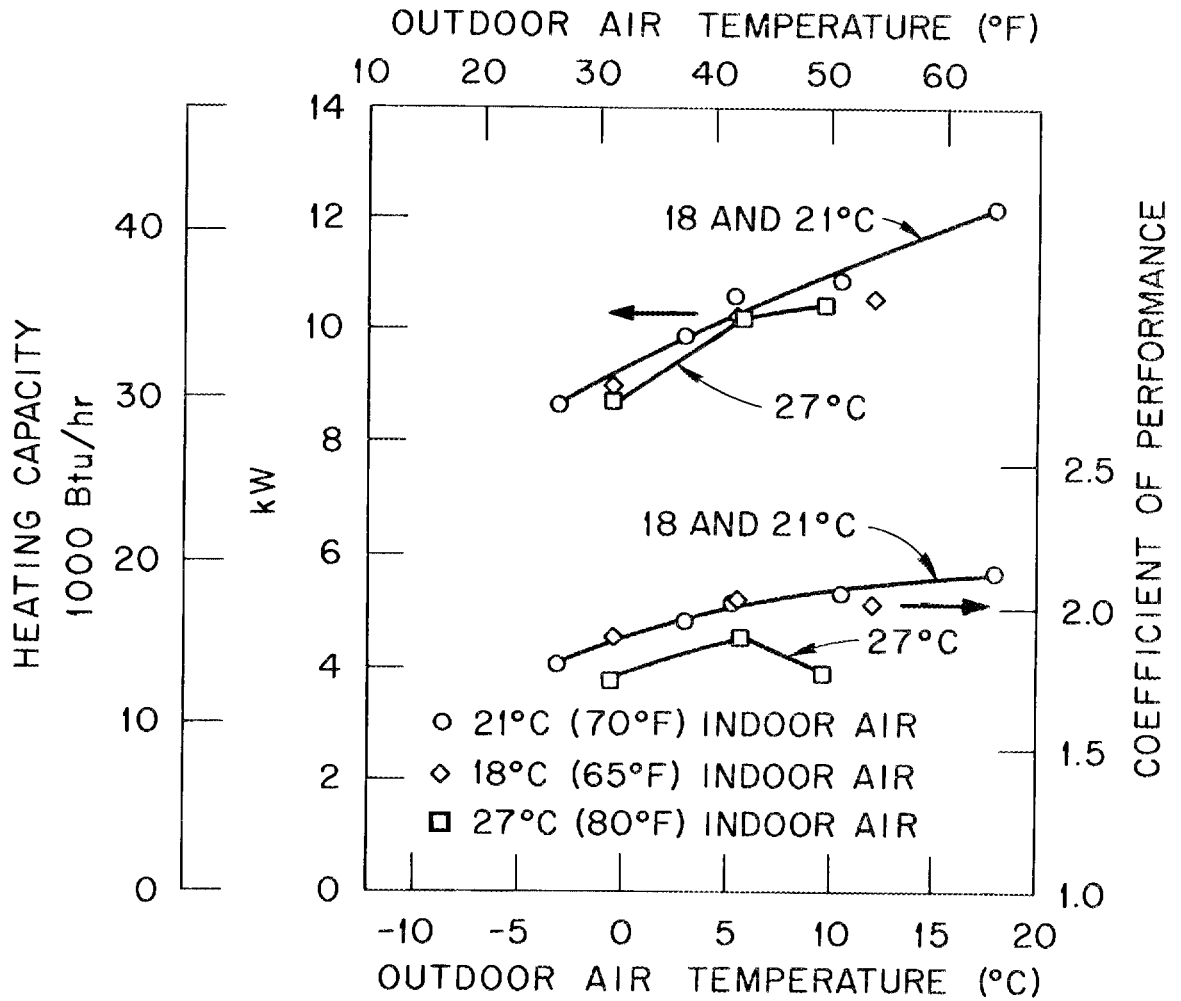


Fig. 6.4. Effect of indoor air temperature on system performance.

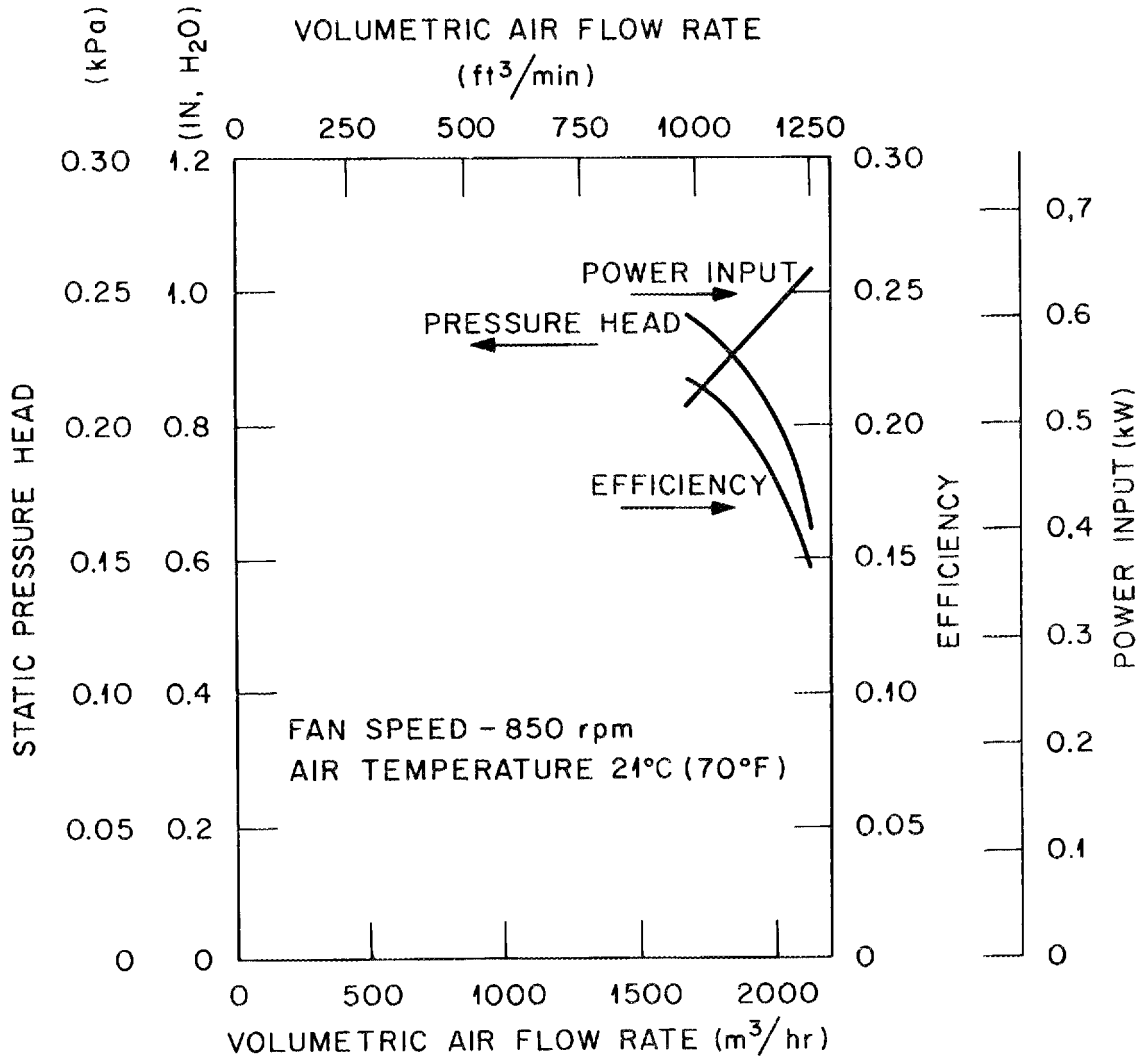


Fig. 6.5. Indoor-fan characteristics.

The nominal flow rate as used in the system is about 2000 m³/hr (1180 cfm); it is apparent, then, that the fan is slightly mismatched to the application as installed in the test loop, and that a fan having similar characteristics and a better match could operate at a higher efficiency. However, the resistance curve of the air system will be influenced not only by the heat-exchanger design and its location in the indoor unit, but also by the resistance generated by the home air-duct network and the air filter. Accordingly, external variables must be considered in evaluating the matching of the fan to the application.

6.2.2 Outdoor-unit fan

The observed outdoor-unit fan and motor characteristics are shown in Fig. 6.6. The peak combined fan and motor efficiency is 0.13 at a flow rate of 3100 m³/hr (1800 cfm), and the efficiency curve is fairly flat. The flow rate as applied is about 4000 m³/hr (2350 cfm); thus it is apparent that the outdoor fan as installed in the test loop also operates at less than peak efficiency in the unfrosted condition, but the penalty in this case is not as great as that for the indoor unit.

In the outdoor unit there is no air ducting, so the air resistance with an unfrosted coil depends solely on the airflow characteristics of the outdoor-unit components as provided by the manufacturer, assuming the contractor follows the installation instructions. However, with frost accumulation the resistance to airflow through the outdoor coil will increase, and the fan must be selected accordingly. Since the efficiency of the outdoor fan of the test unit will increase somewhat as airflow is reduced from the test condition, it appears that operation of the fan in the frosted condition may have been anticipated.

6.2.3 Incentives for improving fan efficiency

Strong economic incentive for increasing the overall efficiency of both air moving devices is apparent. Analysis of this incentive, given below, is typical of the cost-effectiveness analysis that will be applied in future work to other improvements of the heat pump systems.

From Table C.2 (Appendix C), the following values are obtained for the indoor-fan performance:

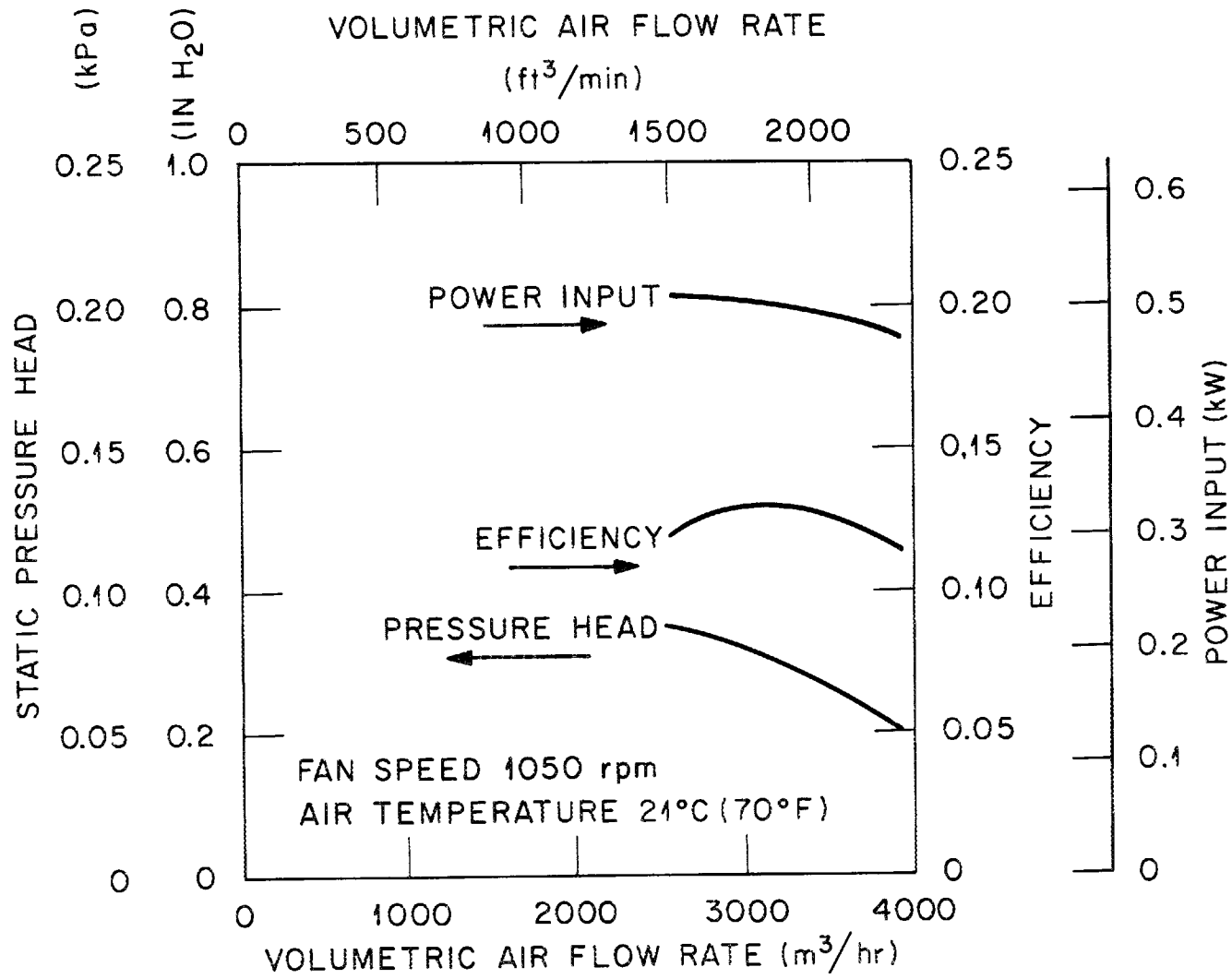


Fig. 6.6. Outdoor-fan characteristics.

Overall efficiency: 16.6% at 2040 m³/hr (1200 cfm)
 Power input: 0.621 kW

If it is assumed that the indoor unit presently incorporates a 65% efficient electric motor and a 25% efficient fan, improving the efficiency of the motor to 70% and the fan efficiency to 30% will result in an overall efficiency of 21%.

If it is further assumed that the average-use cycles are 2080 and 600 heating and cooling load-hours per year respectively,¹ there is a 351-kWhr annual savings realized by the efficiency improvement in the indoor fan-motor unit.

To translate this saving in energy into cost benefit, the following values are assumed:

Present cost of electricity	4¢/kWhr
Yearly rate of escalation of electricity cost	3%
Interest rate available for alternative investment	7%
Assumed useful life of fan-motor unit	10 years

Considering these values, a present worth of \$114 is computed for the energy savings of the improved indoor fan-motor unit. A similar analysis for the outdoor fan-motor unit results in a present worth of \$157. If it is assumed that the improved fans and motors require a \$30 cost increase passed to the buyer of the heat pump, a benefit/cost ratio of 9 is obtained. This is equivalent to a payback period of about one year and, thus, is an attractive investment for the heat pump owner.

6.3 Heat-Exchanger and Capillary-Tube Performance

Performance data that represent the operation of the heat exchangers and capillary tube are presented and discussed together because their operation is interrelated. With a capillary-tube control, refrigerant flow rate through the tube increases both with pressure and subcooling; thus the condensing temperature and pressure for a given operating environment may be elevated to some level by the restriction of flow by the capillary tube regardless of the heat transfer capacity of the condenser.

Operating conditions on the evaporator side are not directly controlled by the capillary tube, and the evaporator naturally assumes a refrigerant temperature-pressure level that allows the volumetric capacity of the compressor to match the flow-rate balance established on the high side. Of course, changes on the low side are reflected on the high side, and vice versa, through their effect on compressor capacity. However, there is no direct control over evaporator exit conditions in a capillary-tube control system.

6.3.1 Condenser (indoor coil)

Table 6.1 shows condenser operating parameters as a function of a range of outdoor air temperatures from -11°C (12°F) to 18°C (64°F). The exit subcooling ranges from 14°C (25°F) at the low ambient to 31°C (56°F) at the high ambient (third column), and the difference between condensing temperature and mean air temperature (fifth column) ranges from 12 – 27°C (22 – 48°F) for the same conditions. The approach of refrigerant exit temperature to inlet air temperature is close: 3.1 – 5.2°C (5.5 – 9.3°F).

It was evident from measurement of return-bend surface temperatures at the indoor coil that the condenser operates about one-half full of liquid, and that the portion of the heat exchanger devoted to condensing is relatively small. Figure 6.7 shows a temperature profile for the indoor coil under three different operating conditions. These data were taken by a hand-held surface thermometer, and, while the values shown probably do not reflect accurate refrigerant temperatures, the shape of the temperature profile is quite clear.

The presence of a large amount of liquid in the condenser is often attributed to an excess of refrigerant charge in the heating mode. We are unable to determine from the test data whether the liquid inventory is the result of an excess charge or the consequence of the capillary-tube characteristics.

Table 6.1. Steady-state indoor-coil (condenser) performance

Outdoor air temperature ^a [°C (°F)]	Condensing temperature ^b [°C (°F)]	Exit subcooling [C° (F°)]	Heat transferred [kW (Btu/hr)]	Mean ΔT refig.-air ^c [C° (F°)]	Minimum ΔT refig. out-air in [C° (F°)]
-11.1 (12.0)	39 (103)	14.1 (25.4)	5.54 (18,900)	12.0 (21.6)	3.1 (5.5)
- 3.1 (26.5)	45 (113)	20.2 (36.4)	7.68 (26,200)	17.0 (30.6)	3.3 (5.9)
3.1 (37.5)	49 (121)	23.1 (41.6)	8.94 (30,500)	19.3 (34.7)	3.8 (6.9)
5.4 (41.7)	51 (124)	24.6 (44.2)	9.41 (32,100)	20.6 (37.1)	4.1 (7.3)
10.6 (51.0)	54 (130)	28.3 (50.9)	10.11 (34,500)	24.3 (43.7)	5.0 (9.0)
17.9 (64.3)	59 (138)	31.3 (56.3)	11.22 (38,300)	26.7 (48.1)	5.2 (9.3)

^aRuns 17, 18, 19, 10, 2, and 1, respectively, as listed in Table B.1. Nominal indoor air temperature is 21°C (70°F).

^bBased on observed high-side pressure and calculated pressure drops in the liquid line and condenser.

^cApproximate value taken as the difference between condensing temperature and mean air temperature.

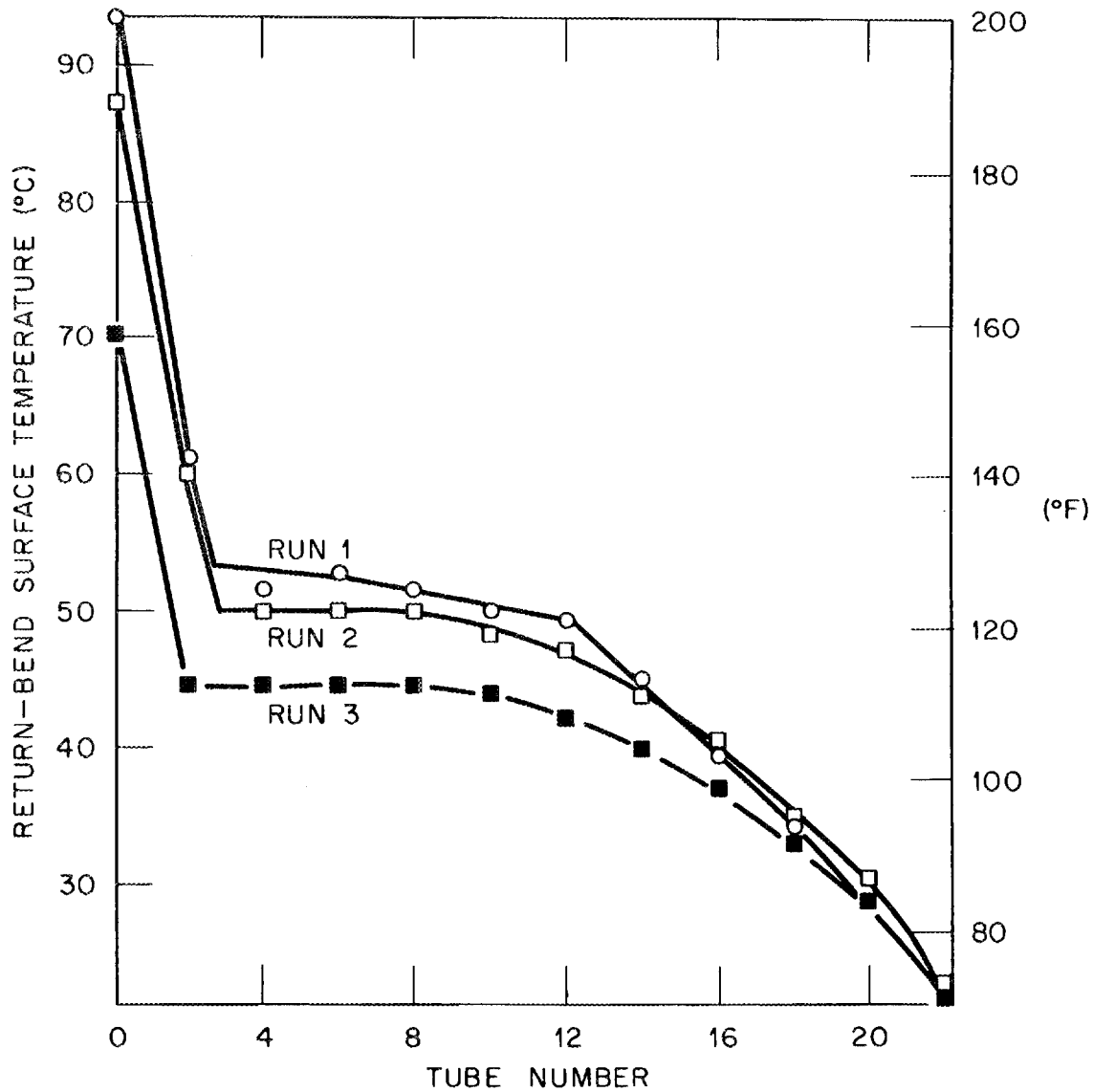


Fig. 6.7. Temperature profile of indoor coil at return bends, operating conditions as follows:

Run	Outdoor air temperature [°C (°F)]	Indoor air temperature [°C (°F)]
1	17.8 (64)	21 (70)
2	10.5 (51)	21 (70)
3	-3.3 (26)	21 (70)

6.3.2 Evaporator (outdoor coil)

Evaporator operating parameters are listed in Table 6.2 for a range of outdoor temperatures. For the -11 and -3°C (12 and 27°F) ambients, the evaporator exit vapor is in the wet saturated region, and the heat transfer rate cannot be computed from refrigerant temperature data. Under these conditions, the evaporating temperature is close to the air temperature (fifth column), leaving little opportunity for superheating. At higher ambient temperatures, the superheat ranges up to 16°C (28°F).

While the differences between evaporating temperature and mean air temperature range from 2 – 12°C (4 – 22°F), the approach of refrigerant exit temperature to air inlet temperature varies in a more complicated manner from 6 – 2°C (11 – 4°F). Achieving the closest approach with the highest heat transfer rate is a surprising result. This is probably attributable to the combined characteristics of the compressor and capillary tube, but at present we have no simple explanation of the way in which evaporator temperatures vary with ambient temperature level.

6.4 System Heat Losses

Two principal sources of heat loss from the system that detract directly from heating capacity were investigated in this study: (1) the compressor shell and (2) the discharge line and reversing valve. In the test system, the compressor is located in the stream of air approaching the outdoor-unit fan; accordingly, there is a brisk flow of air across the uninsulated shell, and conditions for heat loss are ideal. The insulated discharge line experiences an appreciable temperature drop in leading from the compressor discharge in the outdoor unit to the condenser coil in the indoor unit, in spite of the insulation. It appears that a major fraction of this loss occurs at the reversing valve.

These losses, as computed from the test data, are presented in Table 6.3. The apparent compressor heat rejection is large -- over 1.5 kW (5000 Btu/hr). The loss is computed as the difference between electric power input to the compressor and the enthalpy gain of the refrigerant between shell inlet and discharge. While it is possible that temperature

Table 6.2. Steady-state outdoor-coil (evaporator) performance

Outdoor air temperature ^a [°C (°F)]	Evaporating temperature ^b [°C (°F)]	Exit superheat [C° (F°)]	Heat transferred [kW (Btu/hr)]	Mean ΔT air-refrig. ^c [C° (F°)]	Minimum ΔT air in-refrig. out [C° (F°)]
-11.1 (12.0)	-14 (6)	0	- ^d	1.9 (3.5)	3.8 (6.9)
- 3.1 (26.5)	-10 (14)	0	- ^d	4.7 (8.5)	6.1 (11.0)
3.1 (37.5)	- 6 (22)	6 (11)	7.00 (23,900)	5.8 (10.4)	4.1 (7.3)
5.4 (41.7)	- 4 (24)	8 (15)	7.44 (25,400)	6.8 (12.2)	3.2 (5.8)
10.6 (51.0)	- 2 (28)	12 (22)	8.15 (27,800)	8.9 (16.1)	1.9 (3.5)
17.9 (64.3) †	2 (35)	16 (28)	8.94 (30,500)	12.1 (21.8)	2.1 (3.7)

^aRuns 17, 18, 19, 10, 2, and 1, respectively, as listed in Table B.1. Nominal indoor air temperature is 21°C (70°F).

^bBased on observed low-side pressure.

^cInlet air temperature adjusted for fan power input and compressor-shell heat rejection (adjustment estimated for wet-suction conditions). This is an approximate value taken as the difference between mean air temperature and refrigerant evaporating temperature.

^dHeat transfer rate cannot be computed because quality of vapor at evaporator exit is not known.

Table 6.3. System heat losses

Outdoor air temperature [°C (°F)]	Compressor-shell heat rejection [kW (Btu/hr)]	Discharge-line heat loss ^a [kW (Btu/hr)]	Total heat loss [kW (Btu/hr)]	System heat capacity [kW (Btu/hr)]
-11.1 (12.0)	^b	0.15 (500)	—	6.33 (21,600)
- 3.1 (26.5)	^b	0.31 (1060)	—	8.64 (29,500)
3.1 (37.5)	1.61 (5490)	0.32 (1110)	1.93 (6600)	9.87 (33,700)
5.4 (41.7)	1.61 (5490)	0.45 (1550)	2.06 (7030)	10.58 (36,100)
10.6 (51.0)	1.71 (5830)	0.50 (1700)	2.21 (7530)	10.87 (37,100)
17.9 (64.3)	1.66 (5650)	0.65 (2240)	2.31 (7890)	12.16 (41,500)

^aIncludes reversing-valve loss.

^bLoss from compressor shell cannot be computed directly with wet vapor entering the compressor shell, since the quality of the mixture is not known.

measurement errors introduced by refrigerant-line heat conduction close to the compressor tend to exaggerate this apparent loss, it is clear that the loss is substantial. Of course, if the compressor shell were insulated, the refrigerant discharge temperature and the motor temperature would be increased; therefore, it would be necessary to investigate the possibility of compressor overheating before the advisability of providing insulation could be determined.

Some heat-pump manufacturers insulate the compressor for sound reduction, and there will obviously be some attendant thermal benefit. The manufacturer of the test compressor is expected to offer insulation kits in the near future, which could be used to reduce compressor-shell heat loss.

The discharge line of the test system is insulated by a foamed-elastomer sheath approximately 5 mm (3/16 in.) thick. Inspection of the temperature data (Table B.1) leads to the conclusion that most of the discharge-line heat loss occurs at the reversing valve. The computed line loss ranges from 0.15–0.66 kW (500–2240 Btu/hr). It is not clear from the data how much of this loss is rejected to the suction gas at the reversing valve (not considered to be a direct or total loss) or to the ambient air (a direct and total loss).

It is clear, however, that such heat leaks reduce the heating capacity of the system substantially and warrant close attention in the design of high-efficiency systems.

6.5 Compressor Operation

Certain compressor performance parameters are listed in Table 6.4. As would be expected, both power input and refrigerant mass flow rate increase with increasing outdoor air temperature as the result of increased suction-gas density. Also, as would be expected, the pressure ratio decreases as ambient temperature increases, but not substantially. The increased heat-exchanger temperature differences at high ambients tend to maintain the pressure ratio at a high level.

Table 6.4. Compressor operating parameters

Outdoor air temperature [°C (°F)]	Power input [kW (Btu/hr)]	Refrigerant mass flow rate [kg/hr (lb/hr)]	Pressure ratio	Combined motor-compressor efficiency ^a	Volumetric efficiency
-11.2 (12.0)	3.52 (12,000)	101 (223)	4.95	<u> </u> ^b	<u> </u> ^b
- 3.1 (26.5)	3.60 (12,290)	128 (283)	4.81	<u> </u> ^b	<u> </u> ^b
3.1 (37.5)	3.96 (13,500)	142 (312)	4.63	0.40	0.54
5.4 (41.7)	4.09 (13,960)	149 (329)	4.59	0.41	0.55
10.6 (51.0)	4.19 (14,290)	160 (353)	4.57	0.43	0.56
17.9 (64.3)	4.66 (15,900)	174 (384)	4.53	0.44	0.56

^aEfficiency defined as the ratio of ideal isentropic work (between actual shell inlet condition and discharge pressure) to actual electrical power input.

^bCompressor efficiency could not be computed with wet, saturated vapor inlet.

The fifth column of Table 6.4 shows combined motor and compressor efficiency as varying from 0.40 to 0.44 for those conditions at which this parameter could be computed. Efficiency in this case is defined as the ratio of ideal isentropic work, based on observed suction-gas conditions entering the compressor shell and observed discharge pressure, to the actual electrical power input. Accordingly, this efficiency parameter incorporates losses due to motor inefficiency, suction-gas heating, gas throttling losses in the valves and mufflers, mechanical friction, and internal heat transfer into a single value. This parameter should be contrasted to compressor efficiencies computed on the basis of suction-port and discharge-port conditions internal to the shell, since they will be different.

The significance of the 0.40 to 0.44 efficiency-parameter values is that the compressor power input is 2.3 to 2.5 times as much as would be required by a perfect, 100%-efficient compressor. However, since a "perfect" compressor is not achievable, it is not a reasonable basis for comparison. An "excellent" compressor might operate with a motor efficiency of 0.85 and a suction-port to discharge-port isentropic efficiency of 0.75, for a combined efficiency of 0.64. Large open compressors operate at these efficiency levels. On this basis, the test-system compressor power requirement is about 50% greater than that of an "excellent" compressor.

A change in compressor efficiency will not produce the same percent change in system efficiency because the additional energy input resulting from an inefficiency is reflected as an increase in system capacity. That is, if $COP = \text{heat out}/\text{energy in}$, the result of a reduction in inefficiency is:

$$COP = \frac{\text{heat out} - \Delta\text{loss}}{\text{energy in} - \Delta\text{loss}} .$$

Table 6.4 shows the volumetric efficiency of the compressor, based on shell inlet conditions, varying from 0.54 to 0.56. Volumetric efficiency is computed here by the following relationship:

$$\eta_v = \frac{\dot{m}_{ref}}{\rho_s DN} ,$$

where

- η_v = volumetric efficiency,
 \dot{m}_{ref} = observed refrigerant flow rate,
 ρ_s = density of refrigerant vapor entering the compressor shell,
 D = compressor displacement (swept volume),
 N = compressor speed.

7. FROSTING-DEFROSTING TEST RESULTS

7.1 System Performance under Frosting Conditions

The performance of the heat-pump system operating in the heating mode, and subjected to frosting-defrosting conditions, was evaluated at two ambient air dry-bulb temperatures, -3.0 and 2.5°C (26 – 27 and 36 – 37°F), and at one condition of relative humidity, 90–100%.

Tests were conducted initially with 30-min frosting intervals (normally controlled by the cam incorporated by the heat-pump manufacturer) and subsequently with longer frosting intervals. As would be expected, the system performance for the first 30 min of either test is similar; however, there is a difference in the defrost cycle as the frosting period is extended, as will be shown later.

7.1.1 Tests at 2.5°C

Figures 7.1 through 7.5 show the manner in which several of the performance parameters vary during the 90-min frosting interval with the 2 – 3°C (36 – 37°F) outdoor air temperature. Figure 7.1 displays the variation of the heating capacity and COP as a function of the frosting time. The degradation in the heat-pump performance, as manifested by the decrease in both the heating capacity and COP as frost accumulates on the heat exchanger, is the result of the decrease in the volumetric airflow rate across the finned-coil heat exchanger and the thermal resistance of the frost. The decrease in the airflow rate and the corresponding increase in the air pressure drop across the coil are shown as functions of frosting time in Fig. 7.2. The variation in

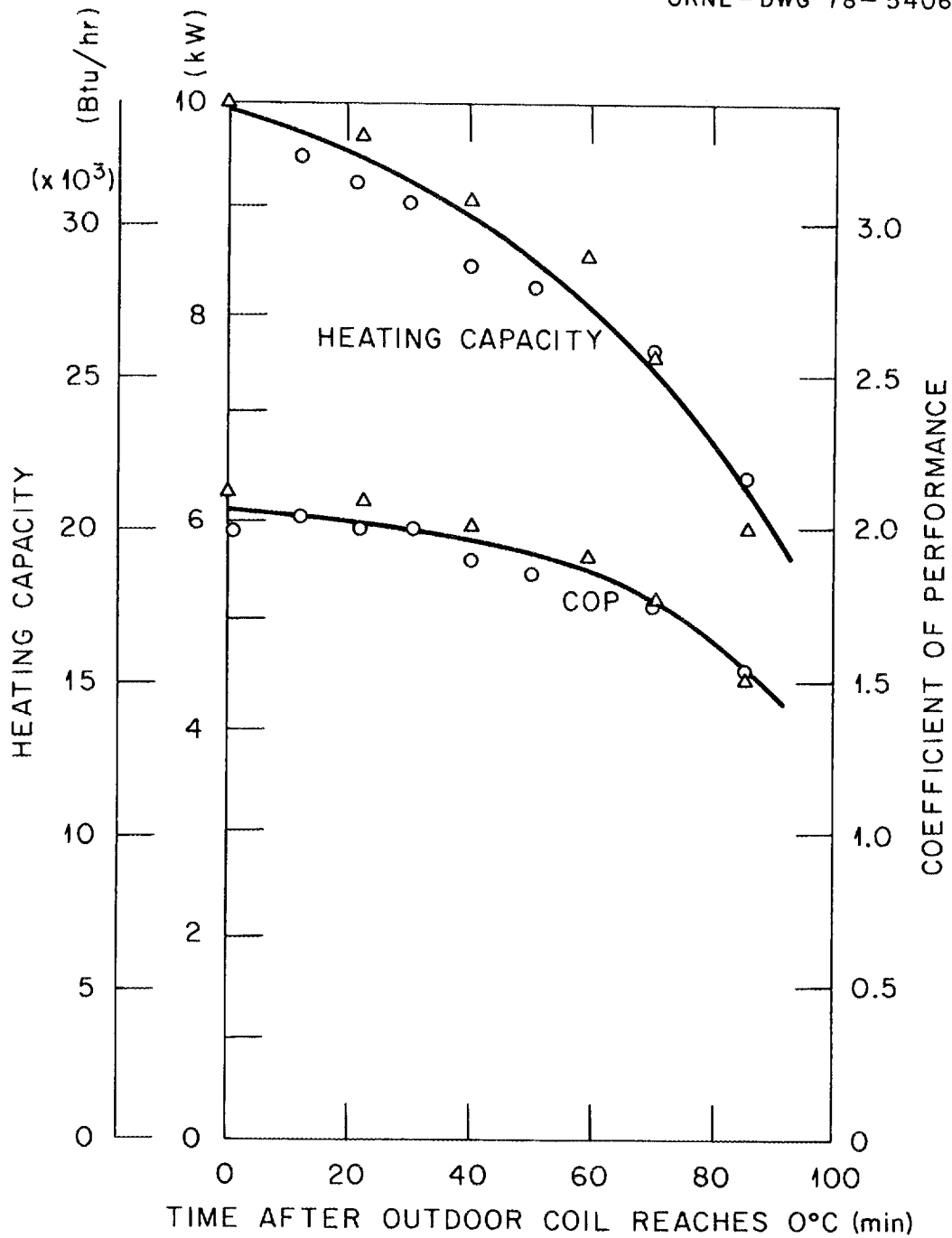


Fig. 7.1. Heating capacity and COP during 90-min frosting period with outdoor air at 2.5°C.

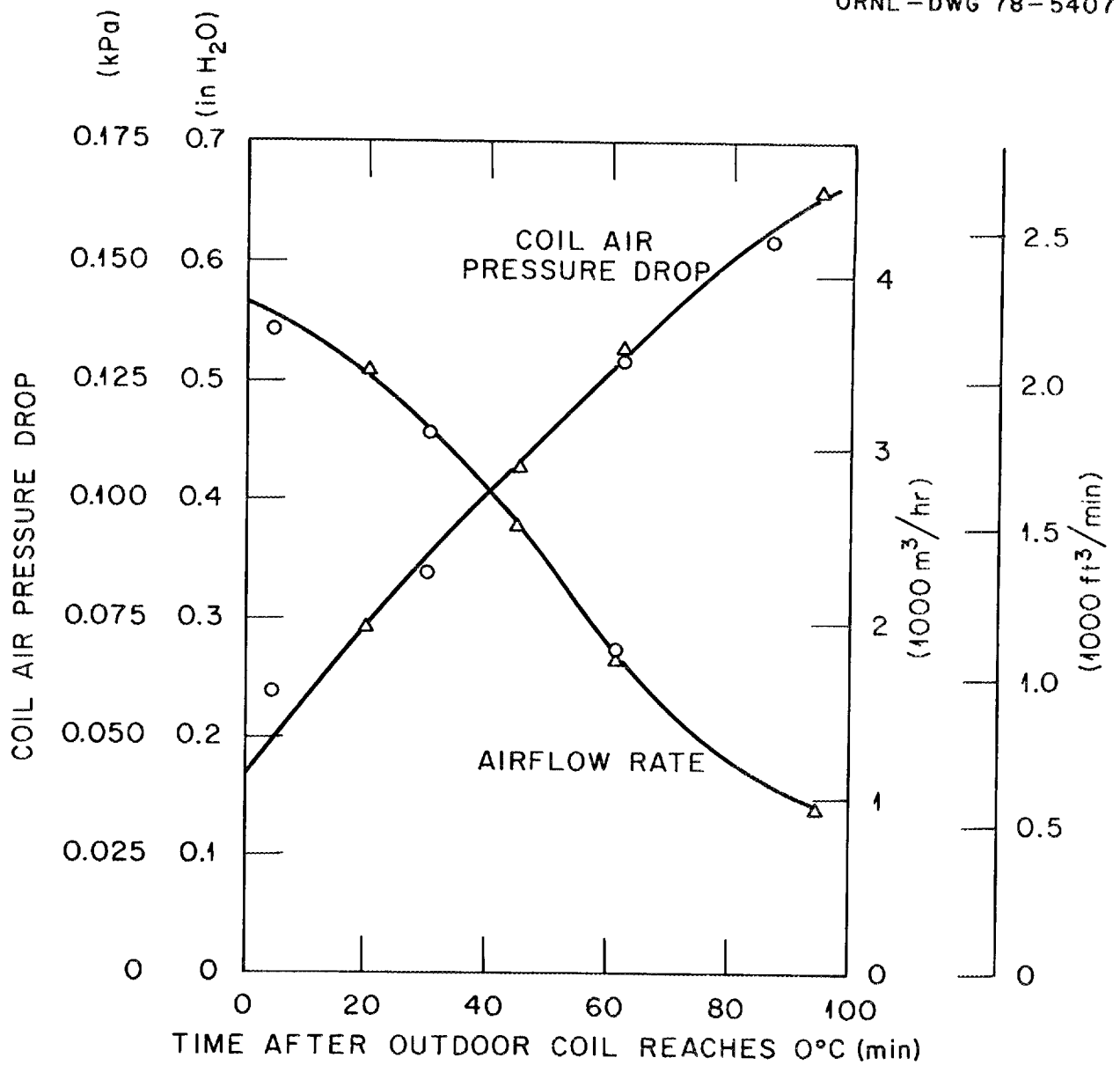


Fig. 7.2. Outdoor-coil air pressure drop and airflow rate during 90-min frosting period with outdoor air at 2.5°C.

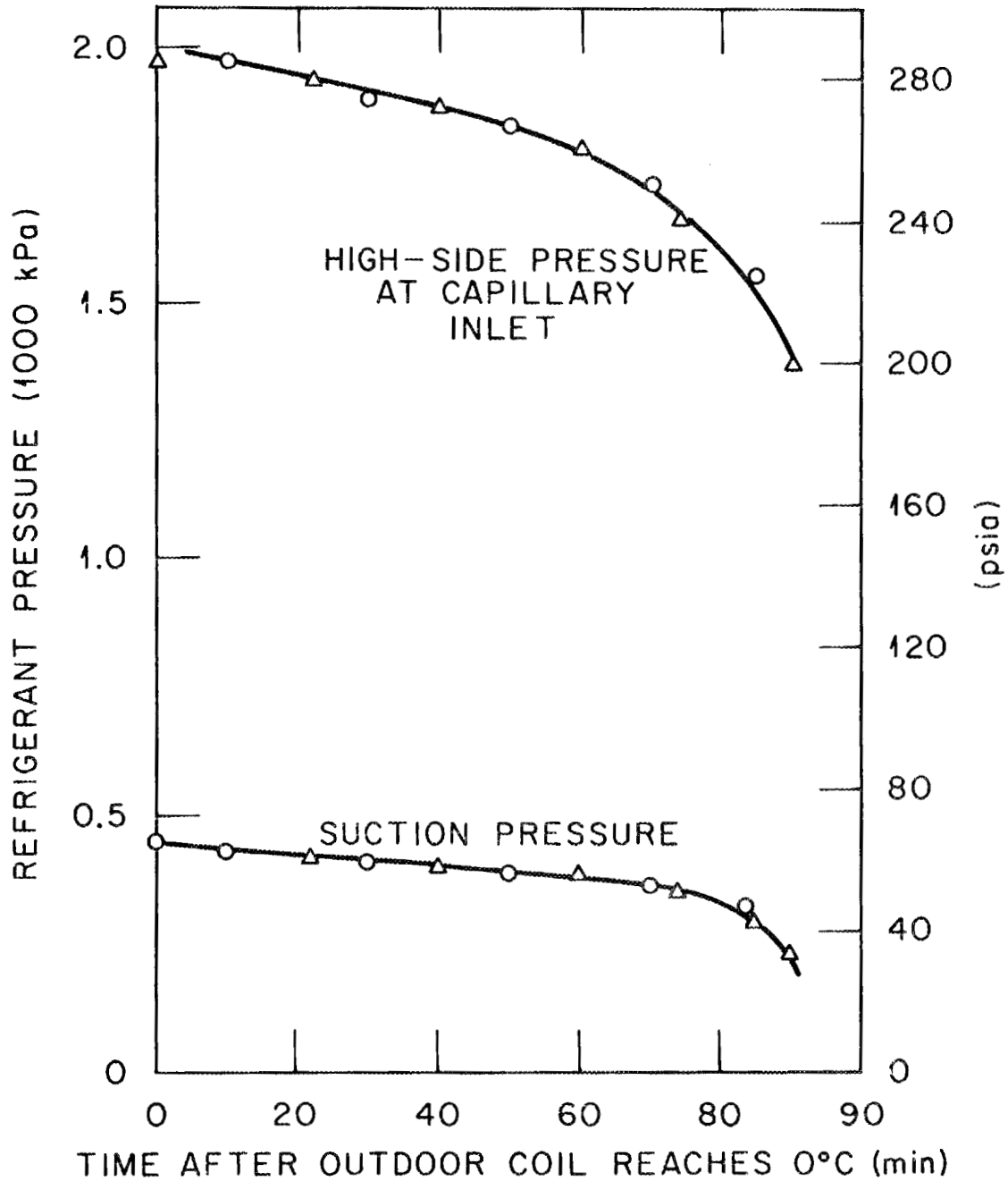


Fig. 7.3. Suction and high-side refrigerant pressure during 90-min frosting period with outdoor air at 2.5°C.

ORNL-DWG 78-5409

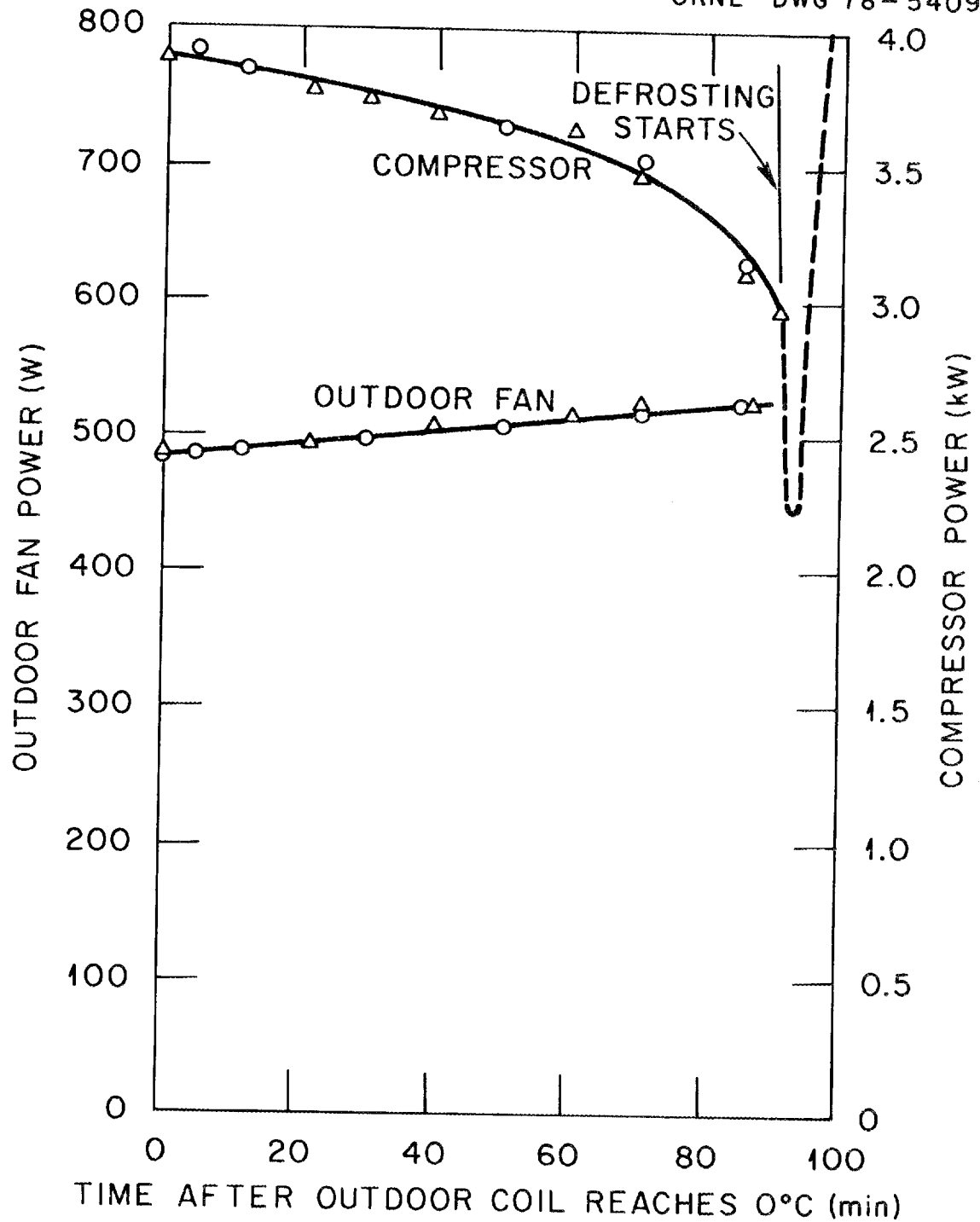


Fig. 7.4. Compressor and outdoor-fan power consumption during 90-min frosting period with outdoor air at 2.5°C.

ORNL - DWG 78-5410

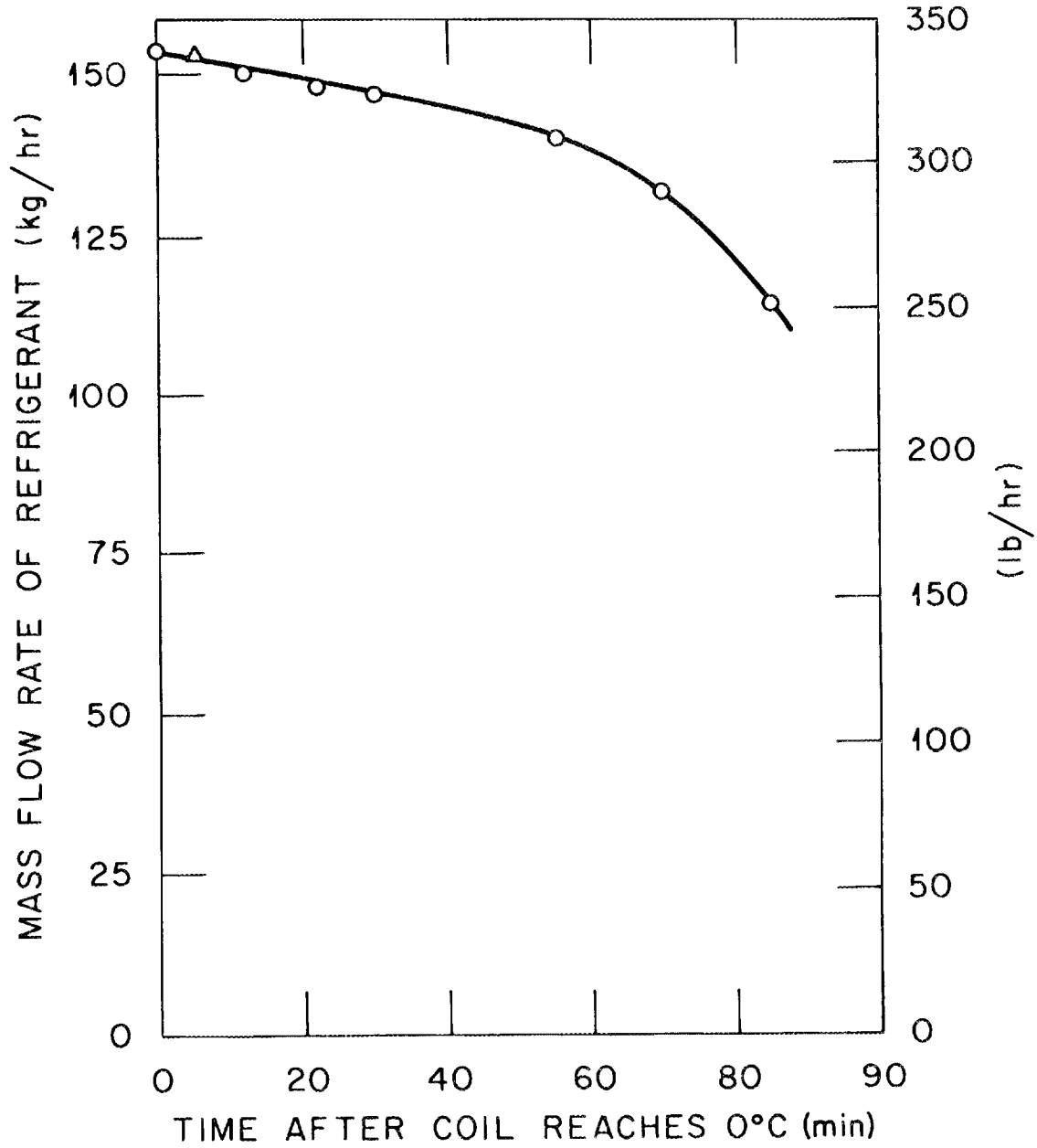


Fig. 7.5. Refrigerant mass flow rate during 90-min frosting period with outdoor air at 2.5°C.

suction and discharge pressure is shown in Fig. 7.3, and the compressor and outdoor-fan power consumption is presented in Fig. 7.4.

Figure 7.5 displays the decrease in mass flow rate of refrigerant as frosting occurs on the outdoor heat exchanger. From 0 to 40 min, there is a linear variation of flow with time. After about 40 min, the frost accumulation affects the mass flow rate of refrigerant more substantially as evidenced by the steep downfall of the curve in the 40- to 90-min interval. Besides a decrease in heating capacity, this refrigerant flow decrease may result in improper cooling of the compressor motor.

After the 30-min frosting period, the outdoor-coil air pressure drop is about doubled, and the airflow is reduced by about 20%. In spite of this, the heating capacity is decreased only 7%, and the COP is down only 3%. Outdoor-fan power has increased about 4% in this period.

After 1 hr of frosting, the heating capacity has dropped by about 20% and the COP by 10%, at which time the outdoor airflow is halved and the coil air pressure drop is tripled. The degradation in system performance is surprisingly small considering the large restriction of the outdoor coil.

After 90 min of frosting, the system performance finally approaches a state of rapid decline. System pressure is dropping rapidly, and performance degradation is extensive. After 90 min of frosting, an approximate 70% decrease in airflow rate has decreased the heating capacity by about 40%, the COP by 30%, the low-side pressure by 45%, the high-side pressure by 33%, and the compressor-motor power by 23%. The outdoor-fan power increase is about 10%.

7.1.2 Tests at -3°C

System performance at the lower frosting temperature, -3°C ($26\text{--}27^{\circ}\text{F}$), is illustrated in Figs. 7.6–7.10. The performance trends are similar to those at $2\text{--}3^{\circ}\text{C}$, except that the rate of degradation in performance is more rapid than at the higher temperature. This is a surprising result, because the absolute humidity is lower at -3°C than

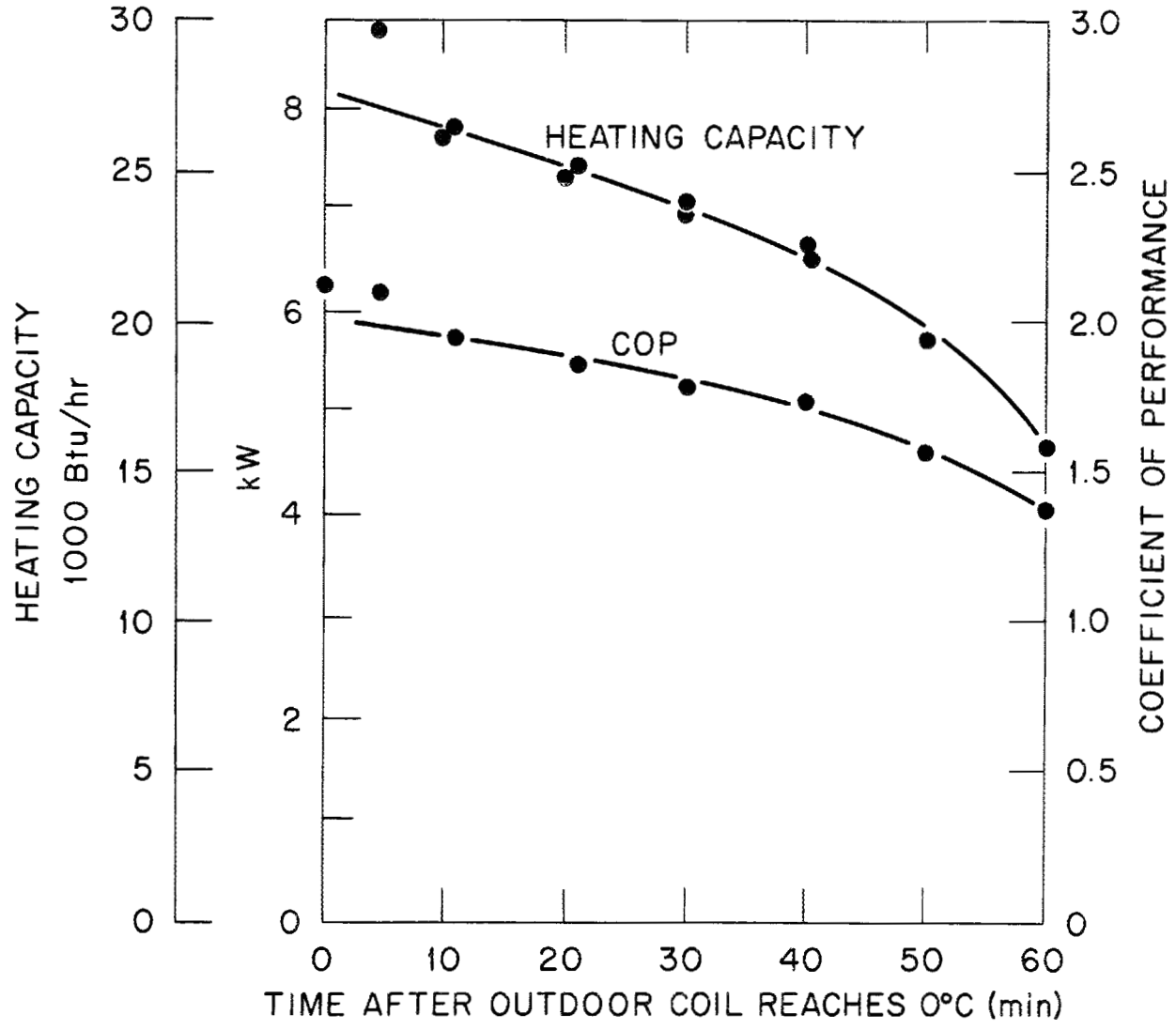


Fig. 7.6. Heating capacity and COP during 60-min frosting period with outdoor air at -3°C .

ORNL-DWG 78-6406

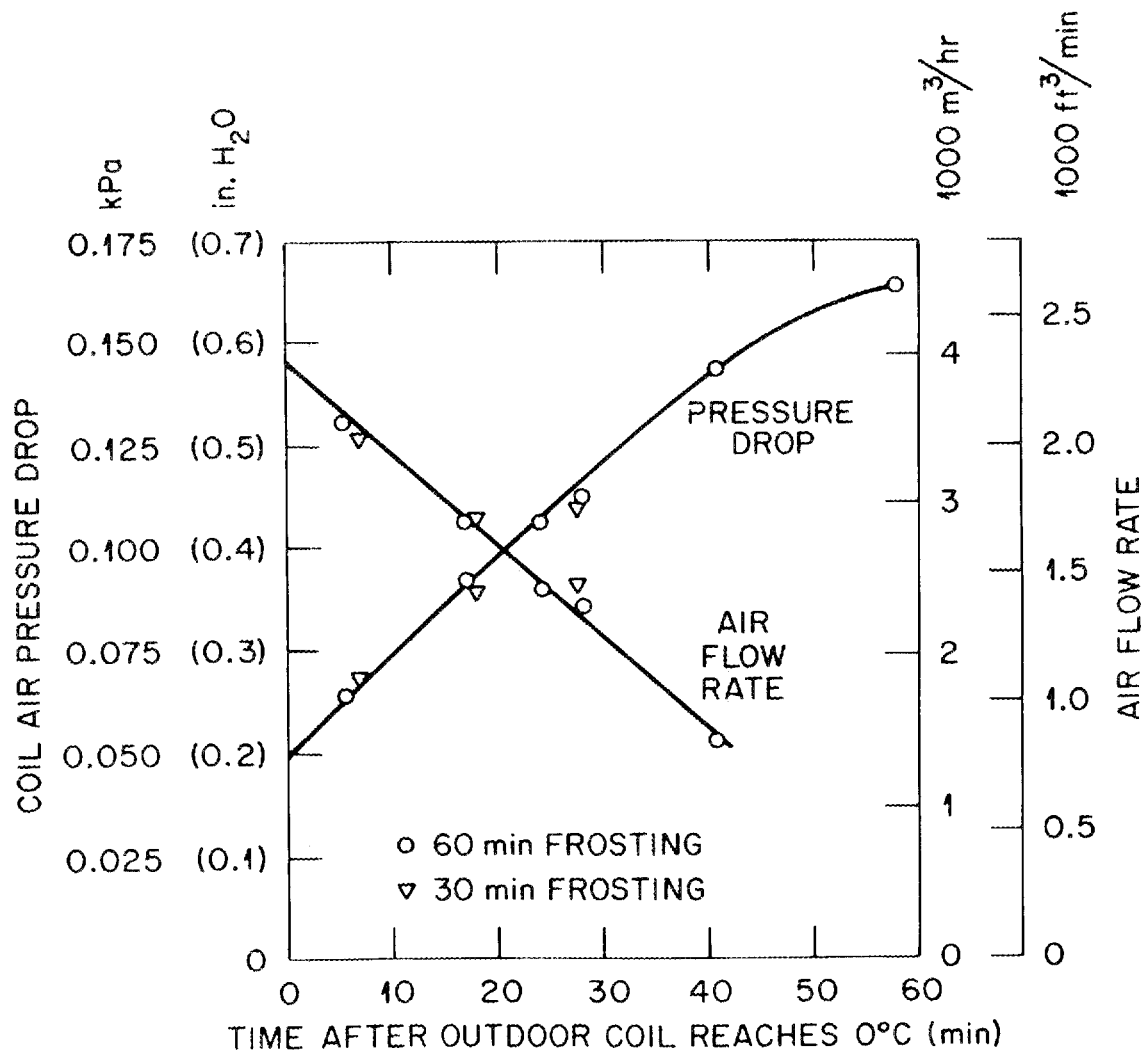


Fig. 7.7. Outdoor coil air pressure drop and airflow rate during 60-min frosting period with outdoor air at -3°C .

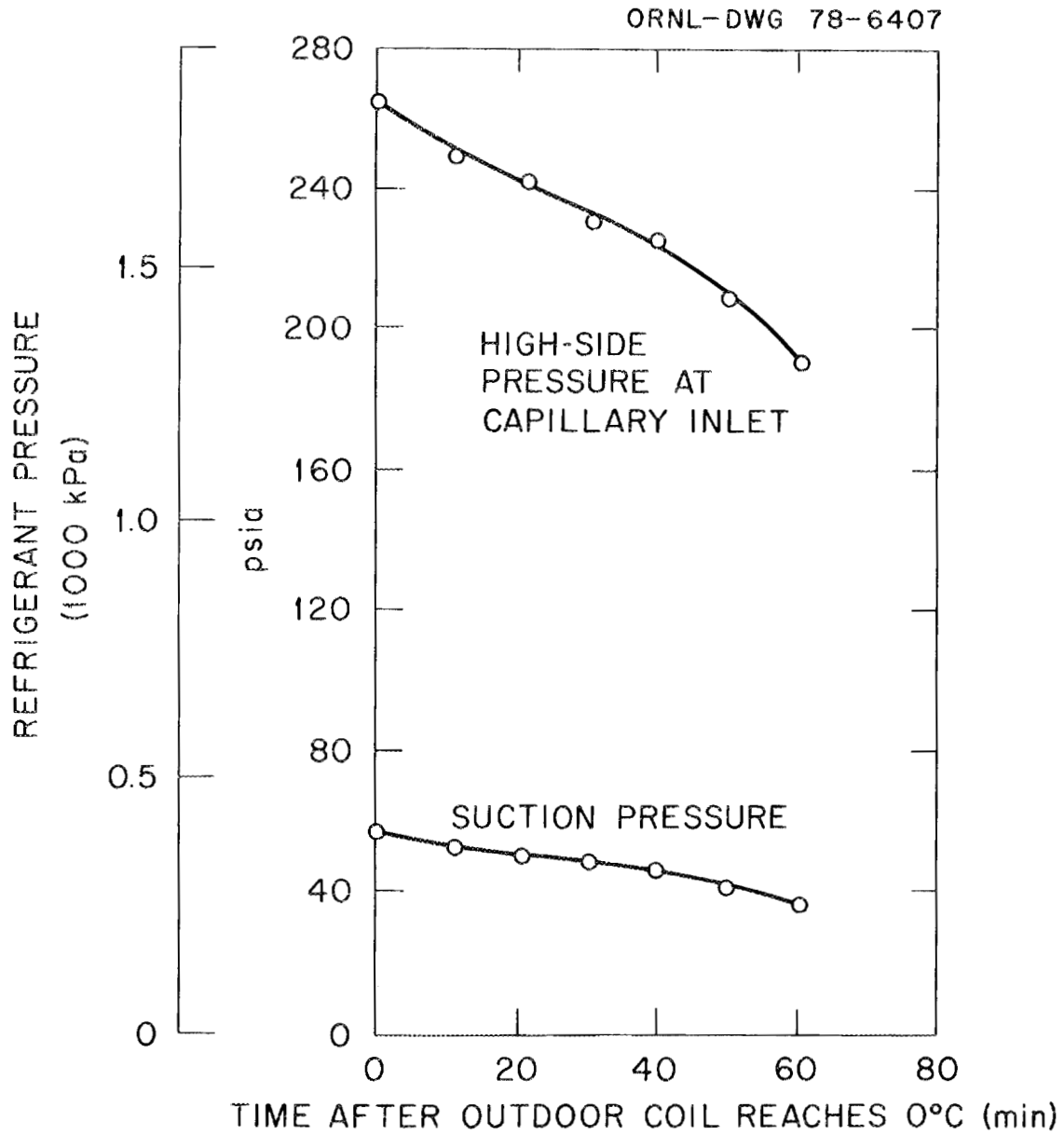


Fig. 7.8. Suction and high-side refrigerant pressure during 60-min frosting period with outdoor air at -3°C .

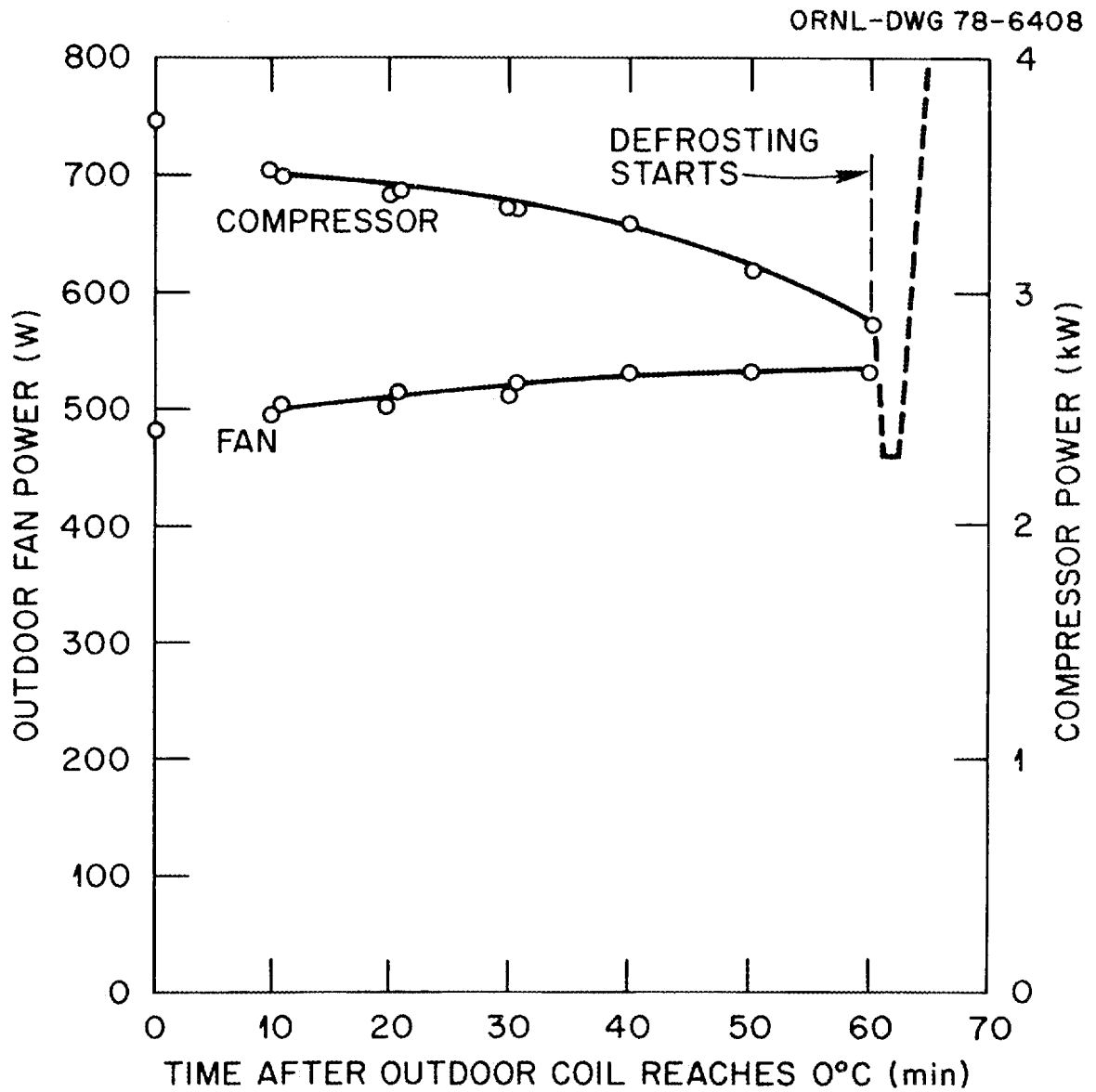


Fig. 7.9. Compressor and outdoor-fan power consumption during 60-min frosting period with outdoor air at -3°C .

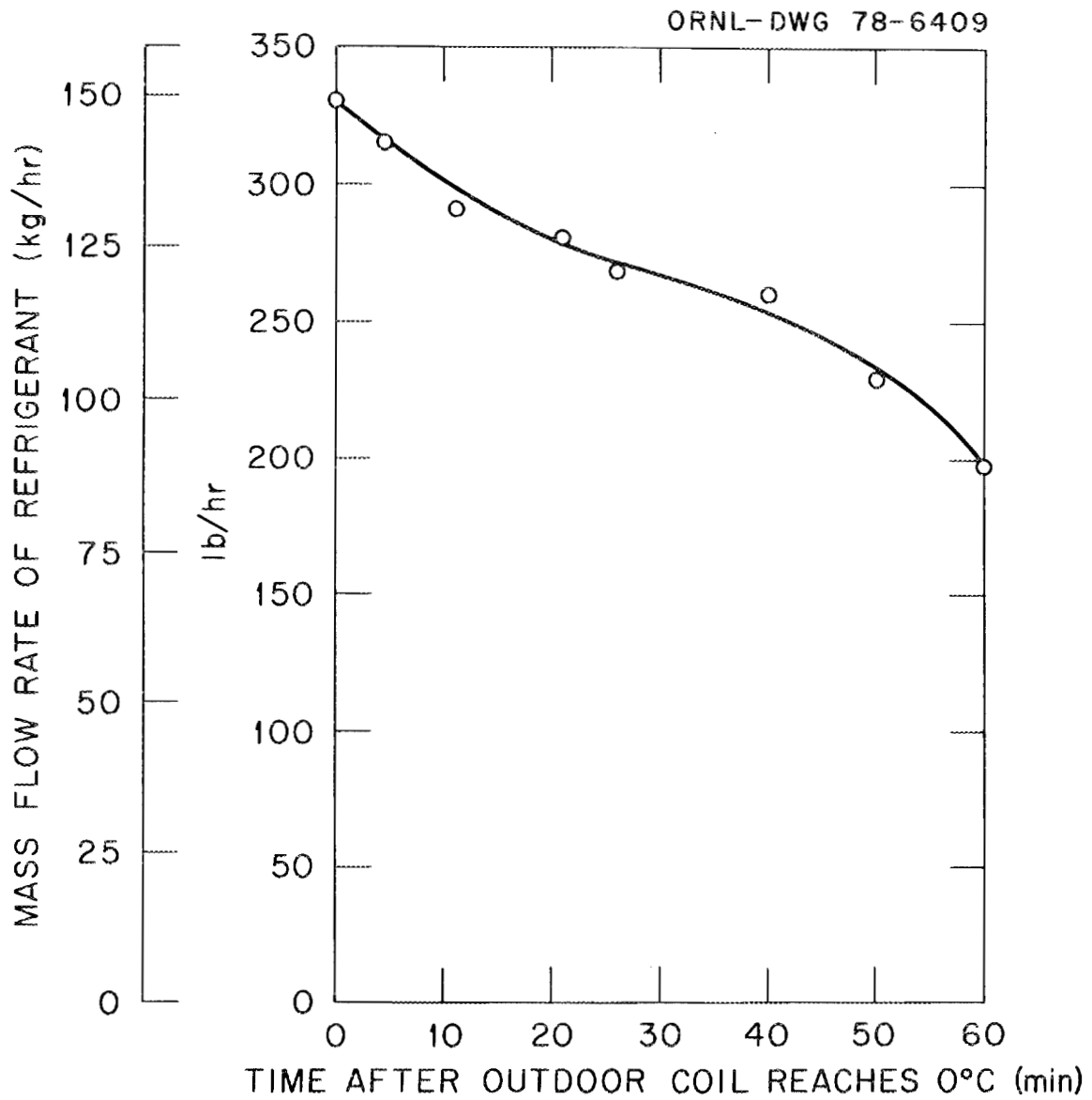


Fig. 7.10. Refrigerant mass flow rate during 60-min frosting period with outdoor air at -3°C .

at 2.5°C. It can be seen from Figs. 7.6–7.10 that the level of performance deterioration reached after 60 min at –3°C was about the same as that observed after 90 min at 2.5°C.

At the end of the 30-min interval, outdoor-coil airflow is halved, the air pressure drop is more than doubled, heating capacity is down 14%, and the COP has dropped 10%.

It should be remembered, of course, that all of the frosting tests in this study were conducted at nearly 100% relative humidity, which is a severe, but not uncommon, operating environment. At lower relative humidity levels, it would be expected that the rate of frosting and system performance degradation would be lower. An investigation of this effect is an appropriate subject for a future investigation.

7.1.3 Defrost water collection

The amount of frost collected on the outdoor coil was measured by collecting the water discharged by the system drain after the defrost period. This method is approximate because there is no control of the residual water on the coil and in the collecting tray. Table 7.1 presents the data for defrost water collected.

Table 7.1. Frost accumulation as approximated by defrost water drain collection

Outdoor air temperature [°C (°F)]	Frosting period (min)	Run No.	Water collected (ml)
2.5 (35–37)	30	1	1200
2.5 (35–37)	30	2	1275
2.5 (35–37)	30	3	1340
2.5 (35–37)	90	4	2850
–3.0 (26–27)	30	1	1000
–3.0 (26–27)	30	2	840
–3.0 (26–27)	30	3	1100
–3.0 (26–27)	60	4	1540

Amounts collected range from 840 to 2850 ml. From these data, it would appear that the higher temperature was the more severe frosting condition as would be expected, but this is contrary to what was concluded in the previous section, where it was apparent that the lower temperature resulted in the greater rate of frost accumulation. Alternatively, it is possible that the pattern form of frost formation varies with temperature or that the amount of water retained on the coil or in the drip pan is a function of temperature.

7.2 Compressor Performance during Defrost Period

During the defrosting interval, four variables were recorded in analog form as a function of time. The values of the compressor-motor and outdoor-fan-motor power (the latter is zero during defrost) and the high- and low-side refrigerant pressures are shown as a function of time after initiation of defrost in Figs. 7.11–7.14. Figures 7.11 and 7.12 show the end of the 30- and 90-min frosting intervals, respectively, and the starting and ending of the defrost interval for outdoor air conditions of 2.5°C (36–37°F) dry-bulb temperature and 90–100% relative humidity.

In Figs. 7.13 and 7.14 are shown the same variables for 30- and 60-min frosting intervals for -3°C (26–27°F) dry-bulb air temperature and 90–100% relative humidity.

Before advancing a brief interpretation of the defrosting effects, described here by these curves and what was observed concurrently at the refrigerant flow meter during the defrosting interval, it is pertinent to notice the similarity of shape between the short frosting intervals (30 min) and the similarity between the long frosting intervals (60 and 90 min). The defrost cycle duration is just under 4 min after 30-min frosting periods at both outdoor temperature levels. For the longer frosting intervals, the defrost cycle lasted over 5 min after 60 min at -3°C (26–27°F) and over 7 min after 90 min at 2.5°C (36–37°F). Some slow oscillations in the system pressures are seen in both defrost cycles after long frosting periods; they are not seen during defrost after 30-min frosting intervals.

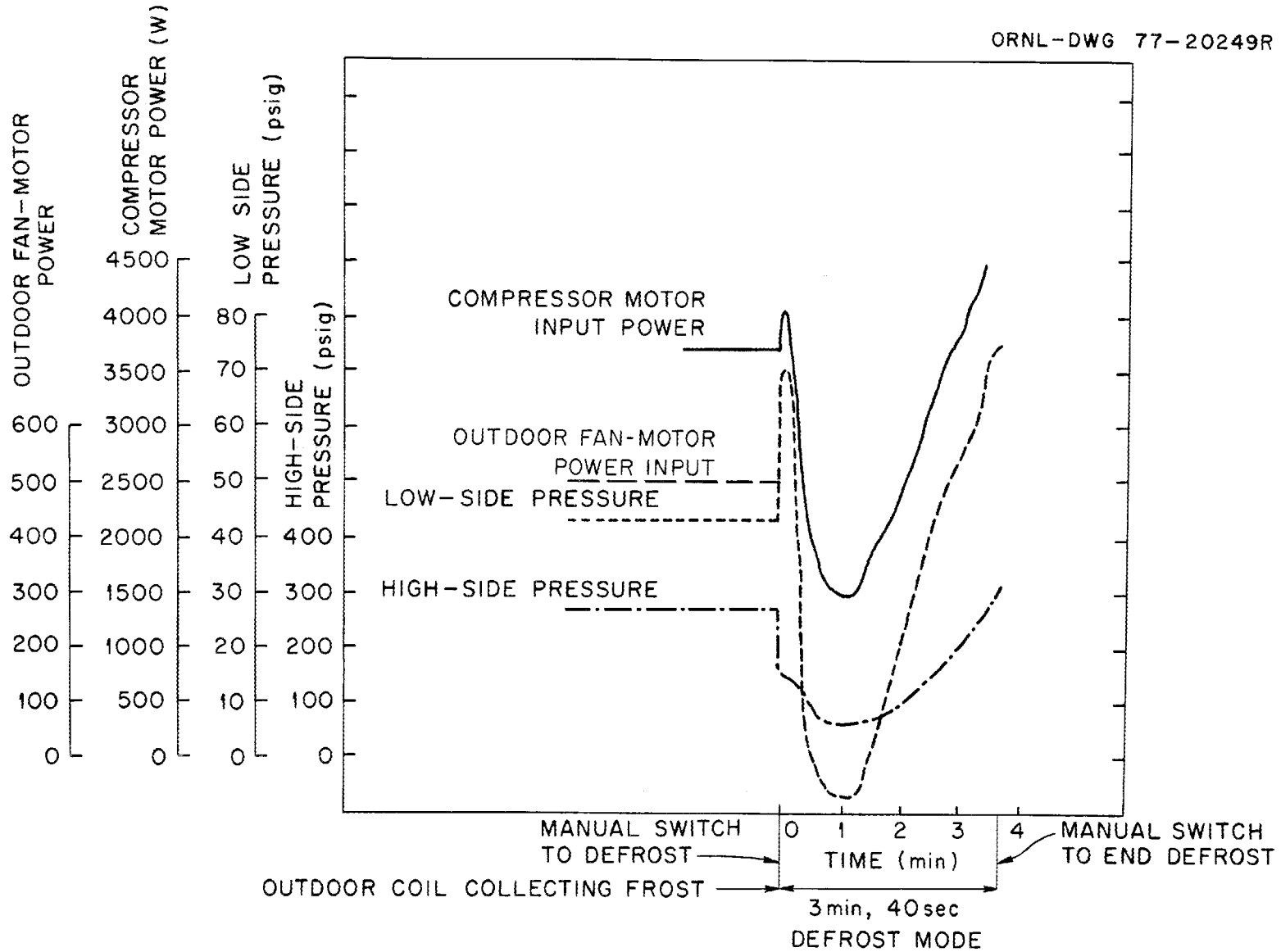


Fig. 7.11. Power consumption and system pressures during defrost period after 30-min frosting with outdoor air at 2.5°C.

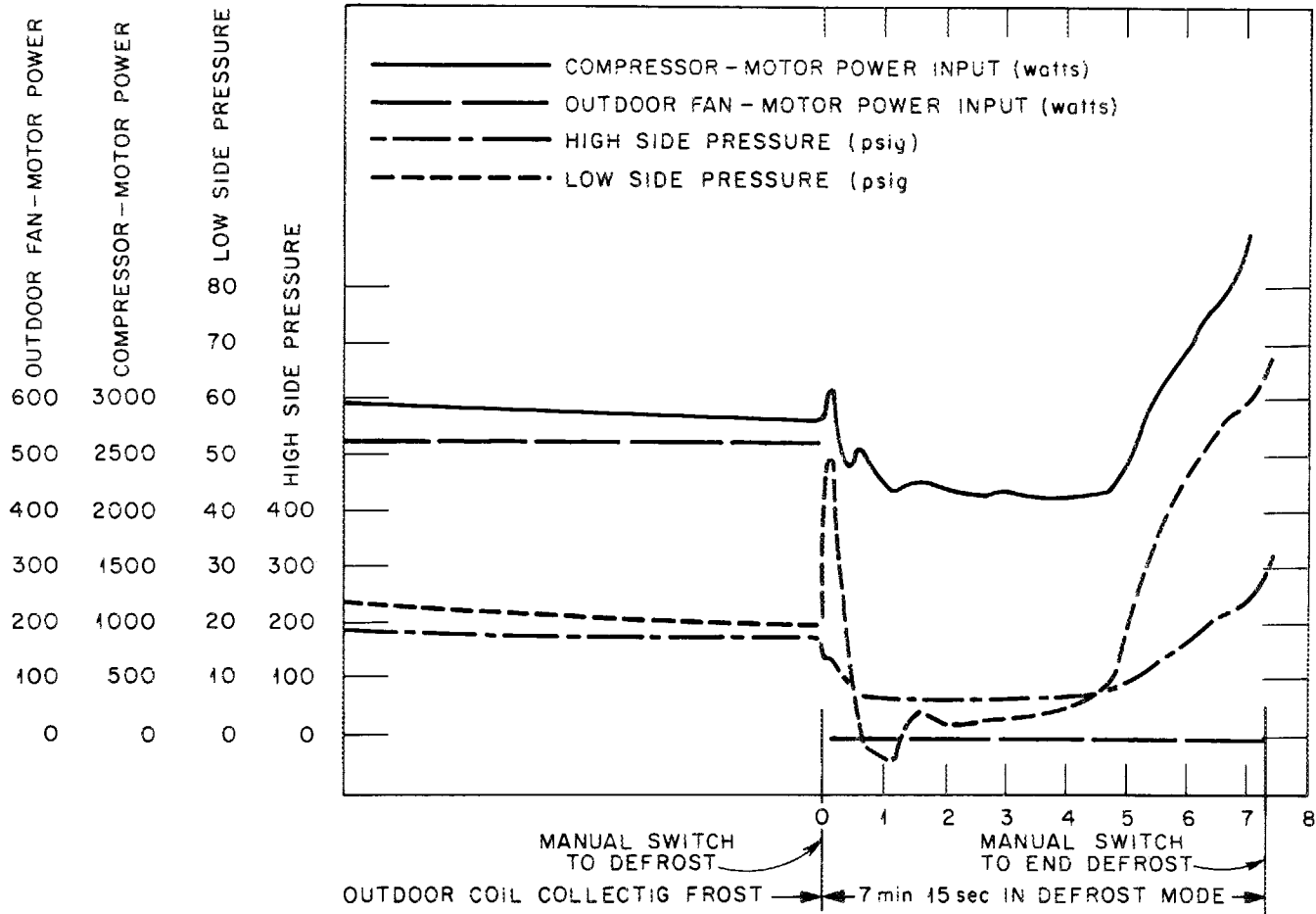


Fig. 7.12. Power consumption and system pressures during defrost period after 90-min frosting with outdoor air at 2.5°C.

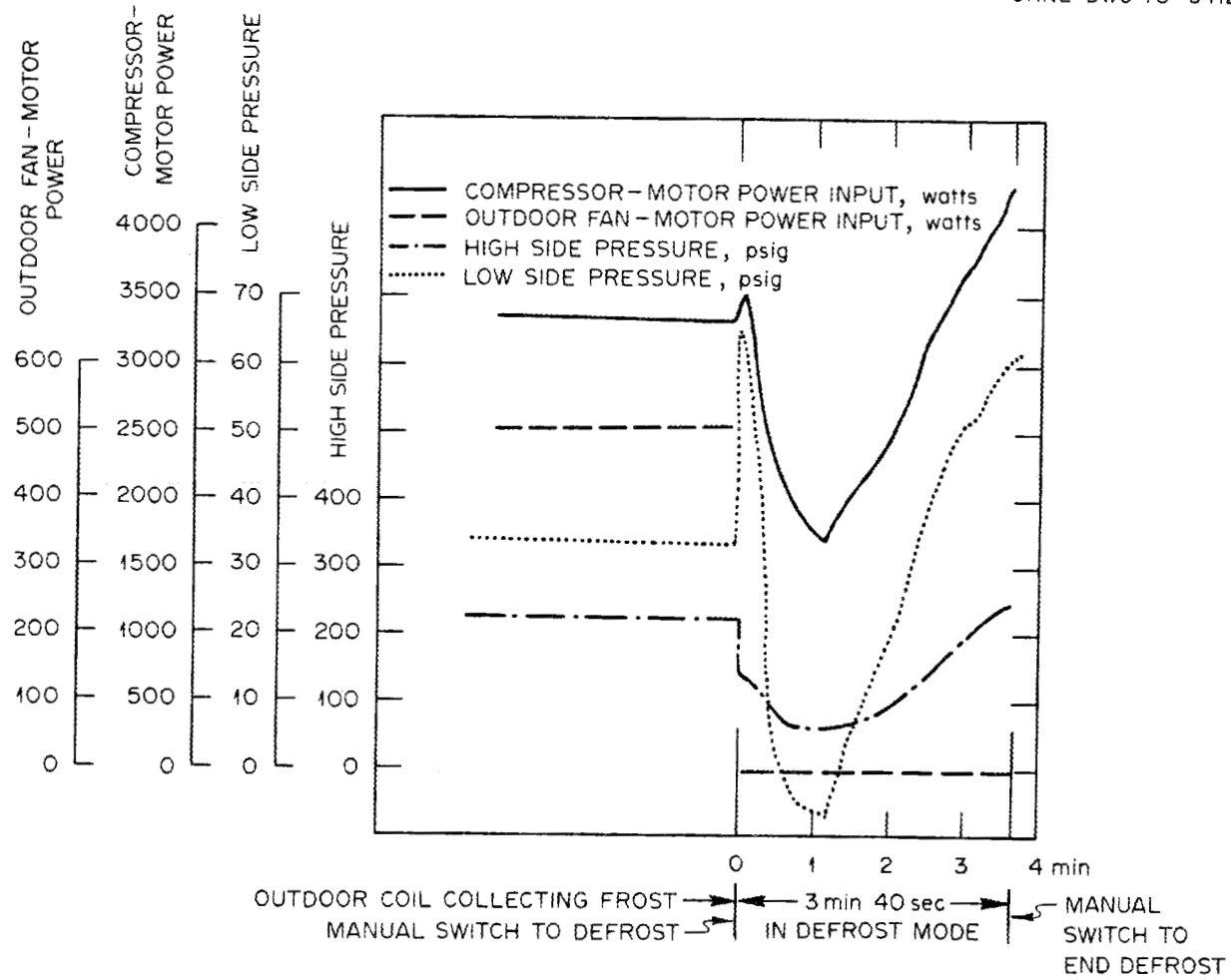


Fig. 7.13. Power consumption and system pressures during defrost period after 30-min frosting with outdoor air at -3°C .

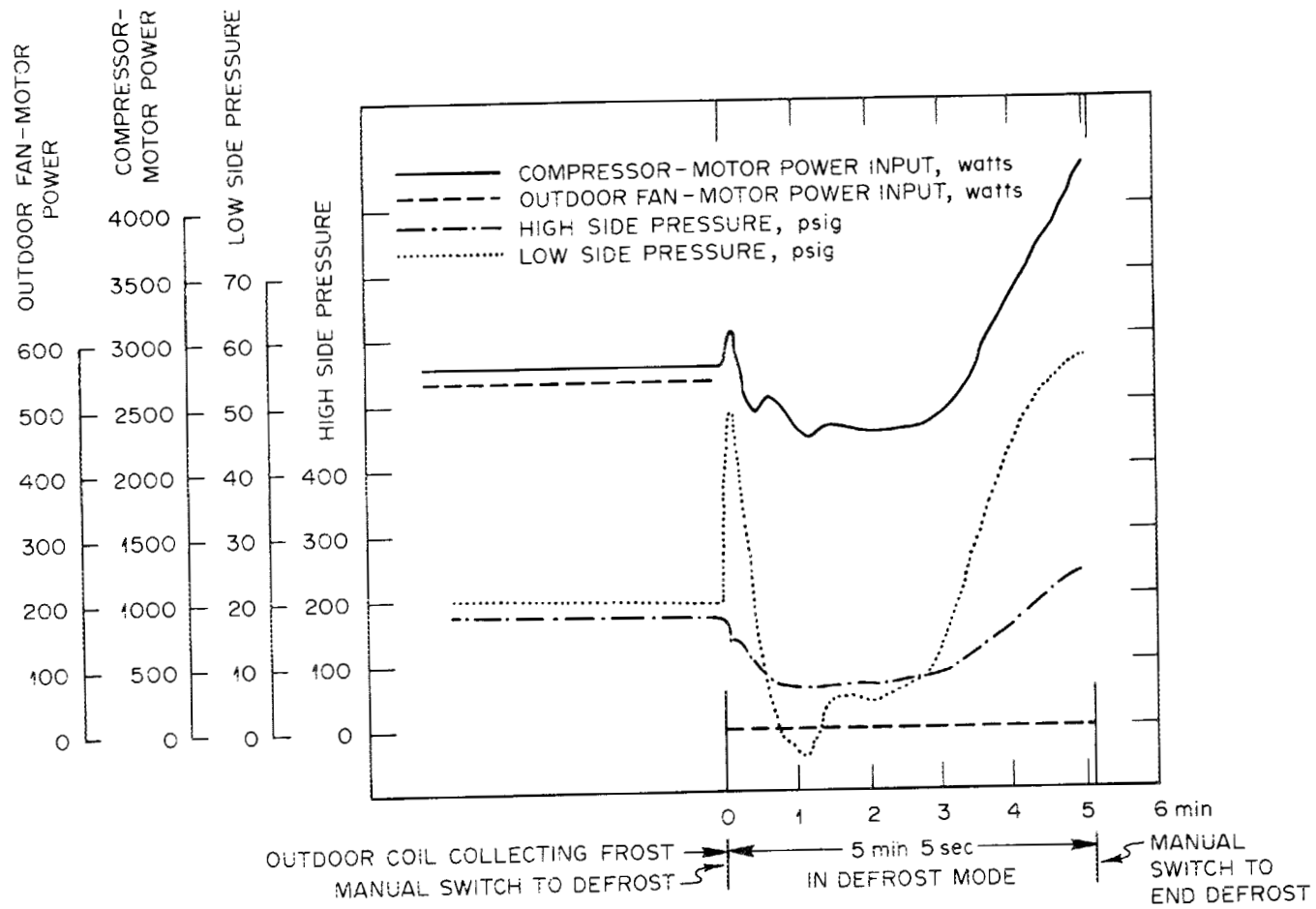


Fig. 7.14. Power consumption and system pressures during defrost period after 60-min frosting with outdoor air at -3°C .

The following interpretation of the strip-chart data for compressor power and system pressures during defrost is carried out for the typical case shown in Fig. 7.11. Just prior to the initiation of defrosting, the indoor-coil contents are about one-half subcooled refrigerant and one-half two-phase refrigerant, while at the outdoor coil there is two-phase refrigerant and some superheated vapor. At the initiation of the defrost, the reversing valve connects the discharge of the compressor to the outdoor coil and the suction side of the compressor to the end of the indoor coil containing superheated gas. Some of the vapor in the indoor coil empties quickly without restriction into the compressor suction, thus causing the observed jump in suction pressure immediately after initiation of the defrost cycle. As the pressure drops in the warm indoor coil, the liquid-refrigerant contents proceed to boil off and pass through the compressor into the cold outdoor coil, where the refrigerant condenses and accumulates. Concurrently, high-side pressure in the liquid line drops as the indoor coil is emptied and the outdoor-coil pressure remains low.

During the first 15 sec after defrosting is initiated, the high-side pressure is seen to drop suddenly from 260 psig to about 140 psig, and the low-side pressure increases from about 40 psig to 70 psig. Afterward the high-side pressure continues decreasing but at a lower rate, and the low-side pressure starts decreasing. Both pressures reached a minimum at about 1 min defrosting time. During this 1-min period the refrigerant-line rotameter float was oscillating while two-phase refrigerant flow, evidenced by bubbles in the rotameter tube, was observed. At the end of this period, the indoor coil has been evacuated to a low (subatmospheric) pressure because high-side pressure has not built up enough to pass refrigerant through to the low side. Compressor power is seen to follow suction pressure during this period.

After about 1 min, observation of the rotameter indicates the resumption of liquid refrigerant flowing through it. The rotameter float rises steadily in the liquid in this portion of the defrost cycle, as normal functioning as a vapor-compression system is resumed. The system pressures begin to increase rapidly and approach an overload condition

because of the stopped outdoor fan. The outdoor-coil temperature sensor terminates the defrost cycle before the overload condition is reached.

At the termination of the defrost cycle and resumption of the heating mode, a transient in system operating conditions is experienced, which appears to last no more than 1 min.

7.3 Average COP for the Frosting-Defrosting Cycle

For ambient conditions under which frosting will occur, an average COP over the frosting-defrosting cycle is the significant measure of system efficiency. A proper method of evaluating COP for the frosting-defrosting cycle would seem to depend upon whether the system were operating above or below the balance point.* If the system is operating at ambient temperatures below the balance point, the loss in capacity during frosting must be replaced by resistance heat. Therefore, constant heating output with supplementary resistance heat appears to be a fair basis for determining average COP under these conditions.

For operation above the balance point, no additional resistance heat would be needed; therefore, an average COP without supplemental heat seems an appropriate measure for this case. Calculations were performed to determine an average effective COP under both sets of conditions.

Computed values for average COP are shown in Table 7.2, contrasted with the COP at the beginning of the frosting period. Average values are computed assuming that compressor power input during defrost is lost from the system. Average COP values were computed using the following expressions:

$$\text{COP} = \frac{\left(\dot{q}_{\text{pump heat}} + \dot{E}_{\text{res. heat}} \right) \text{ avg. over } \Delta\tau_{\text{frosting interval}} + \left(\dot{E}_{\text{res. heat}} \right) \text{ avg. over } \Delta\tau_{\text{defrost period}}}{\left(\dot{E}_{\text{pump heat}} + \dot{E}_{\text{res. heat}} \right) \text{ avg. over } \Delta\tau_{\text{frosting interval}} + \left(\dot{E}_{\text{pump heat}} + \dot{E}_{\text{res. heat}} \right) \text{ avg. over } \Delta\tau_{\text{defrost period}}}$$

*Balance point is defined as the outdoor dry-bulb temperature at which heat-pump capacity exactly matches building heating load.

Table 7.2. Average COP over frosting-defrosting cycle

Outdoor air temperature [°C (°F)]	Frosting interval (min)	Defrost interval (min)	COP, no-frost	Average COP, frost-defrost cycle	Average COP with supplementary electric heat
2.5 (36-37)	30	3.7	2.05	1.73	1.60
2.5 (36-37)	90	7.3	2.05	1.69	1.48
-3 (26-27)	30	3.7	2.00	1.56	1.42
-3 (26-27)	60	5.1	2.00	1.47	1.33

for the case where the system is penalized for the use of supplementary resistance heat; for the case in which resistance heat is not used,

$$\text{COP} = \frac{\dot{q}_{\text{heat pump, avg. over frosting interval}} \Delta\tau_{\text{frosting}}}{\dot{E}_{\text{heat pump, avg. over frosting interval}} \Delta\tau_{\text{frosting}} + \dot{E}_{\text{heat pump, avg. during defrost period}} \Delta\tau_{\text{defrost}}}$$

In the above expressions,

\dot{q} = heating capacity,

\dot{E} = energy input,

$\Delta\tau$ = time duration.

For the 2.5°C (36-37°F) outdoor air condition, the average COP with a 30-min frosting period is 1.73 without supplementary resistance heat and 1.60 with supplementary heat: 84 and 78% of the unfrosted COP respectively. At the -3°C (26-27°F) condition and a 30-min frosting interval, the average COP values are 1.66 and 1.42: 78 and 71% of the unfrosted conditions.

The values in Table 7.2 illustrate that a 30-min frosting period is more energy efficient than the 60- and 90-min periods. However, there are not sufficient data to determine whether the manufacturer's 30-min timing is optimum for best efficiency. This could be the subject of a future research study.

8. REFRIGERANT CHARGE VARIATION TESTS

Figure 8.1 shows the manner in which system refrigerant pressures vary with refrigerant charge. Tests were conducted with 10°C (50°F) outdoor air and 21°C (70°F) indoor air temperatures. Pressures are seen to be approximately proportional to refrigerant charge in the undercharge condition, and to level off somewhat in the overcharge range. Undercharge tests were terminated when bubbles were observed in the liquid line, at about 1.8 kg (4 lb) charge, indicating incomplete condensation. As would be expected, the evaporating temperature decreased as charge and suction pressure decreased. This leads to an increasing level of superheat at the evaporator exit, as shown in Fig. 8.2. Superheat drops rapidly with increasing charge in the overcharge range, dropping to zero in some of the tests.

Refrigerant mass flow rate is highly sensitive to refrigerant charge, as shown in Fig. 8.3. The steep drop in mass flow rate as charge is reduced is the consequence of both dropping suction pressure and rising suction superheat.

Figure 8.4 shows the variation in heating capacity with charge; the shape of this curve is seen to be similar to that of the mass flow rate curve (Fig. 8.3) as would be expected since capacity is equal to the product of refrigerant flow rate and enthalpy difference.

The effect of charge on COP is shown in Fig. 8.5. The COP is essentially constant in the overcharge range and drops off in the undercharge range, but less sharply than heating capacity and refrigerant mass flow rate.

As has been pointed out previously in this report, the test system did not employ a suction-line accumulator, while most, if not all, currently manufactured heat pumps do use an accumulator. In fact, current-year models of the test system have an accumulator. Since the use of a suction-line accumulator can be expected to alter the charge sensitivity characteristics of a system, the performance changes presented here should not be considered representative of current systems. Comparison with future test data for another system may indicate the benefits in reduced charge sensitivity that accrue from the use of a suction-line accumulator.

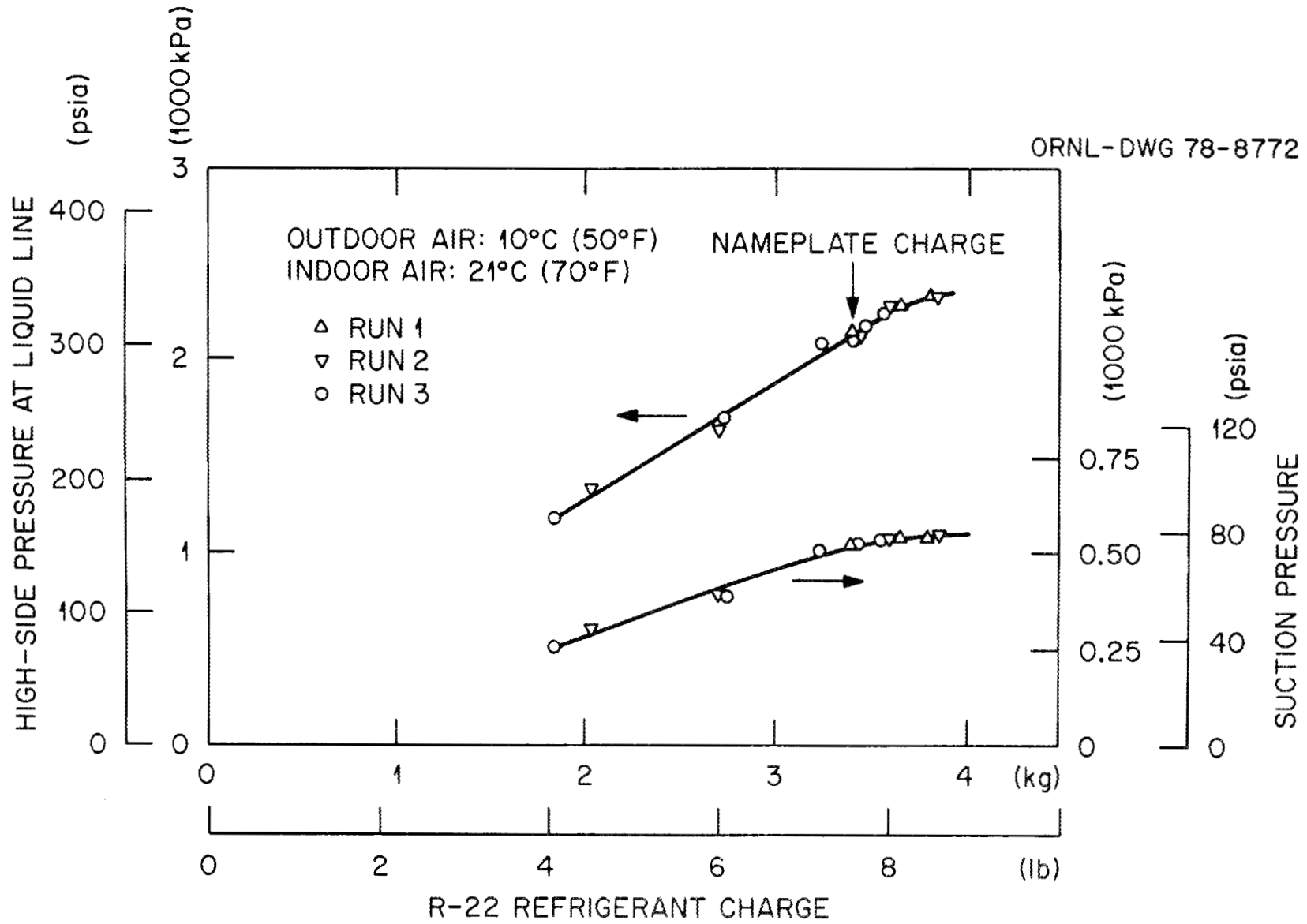


Fig. 8.1. High-side and suction-side pressures as functions of refrigerant charge.

ORNL-DWG 78-8773

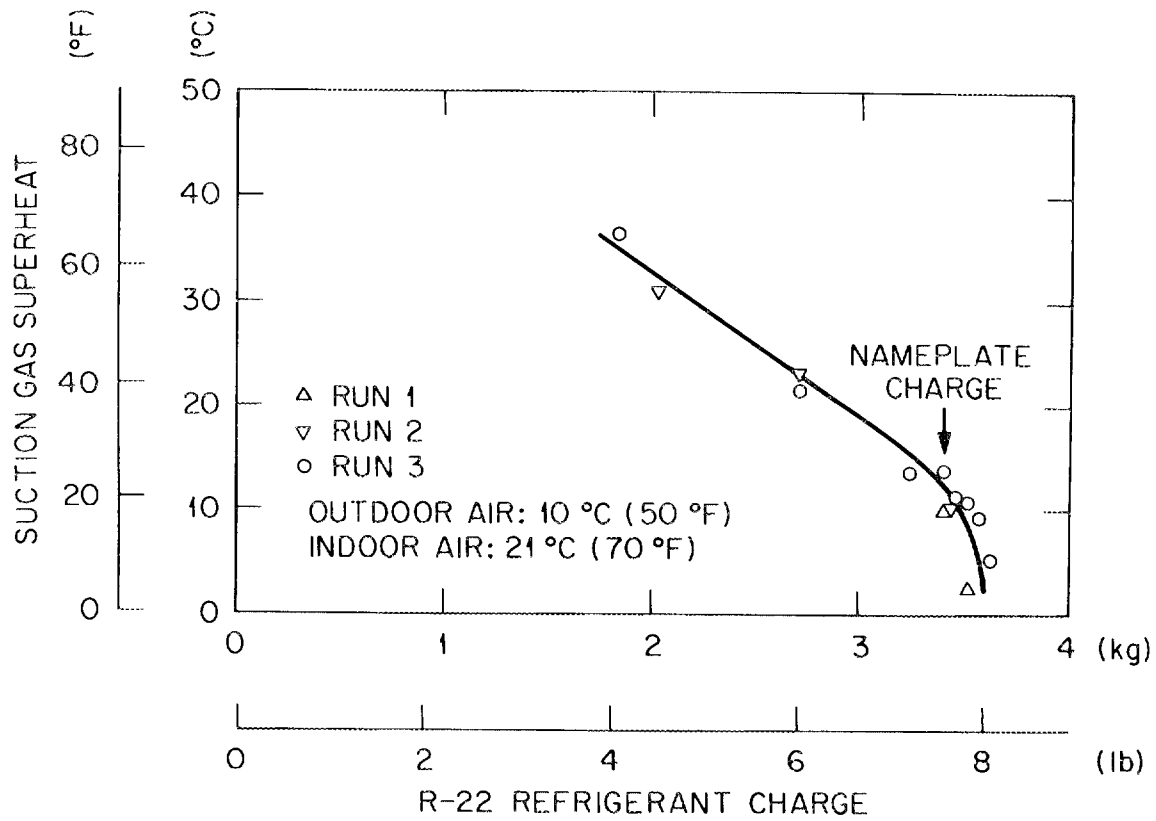


Fig. 8.2. Suction gas superheat as a function of refrigerant charge.

ORNL-DWG 78-8775

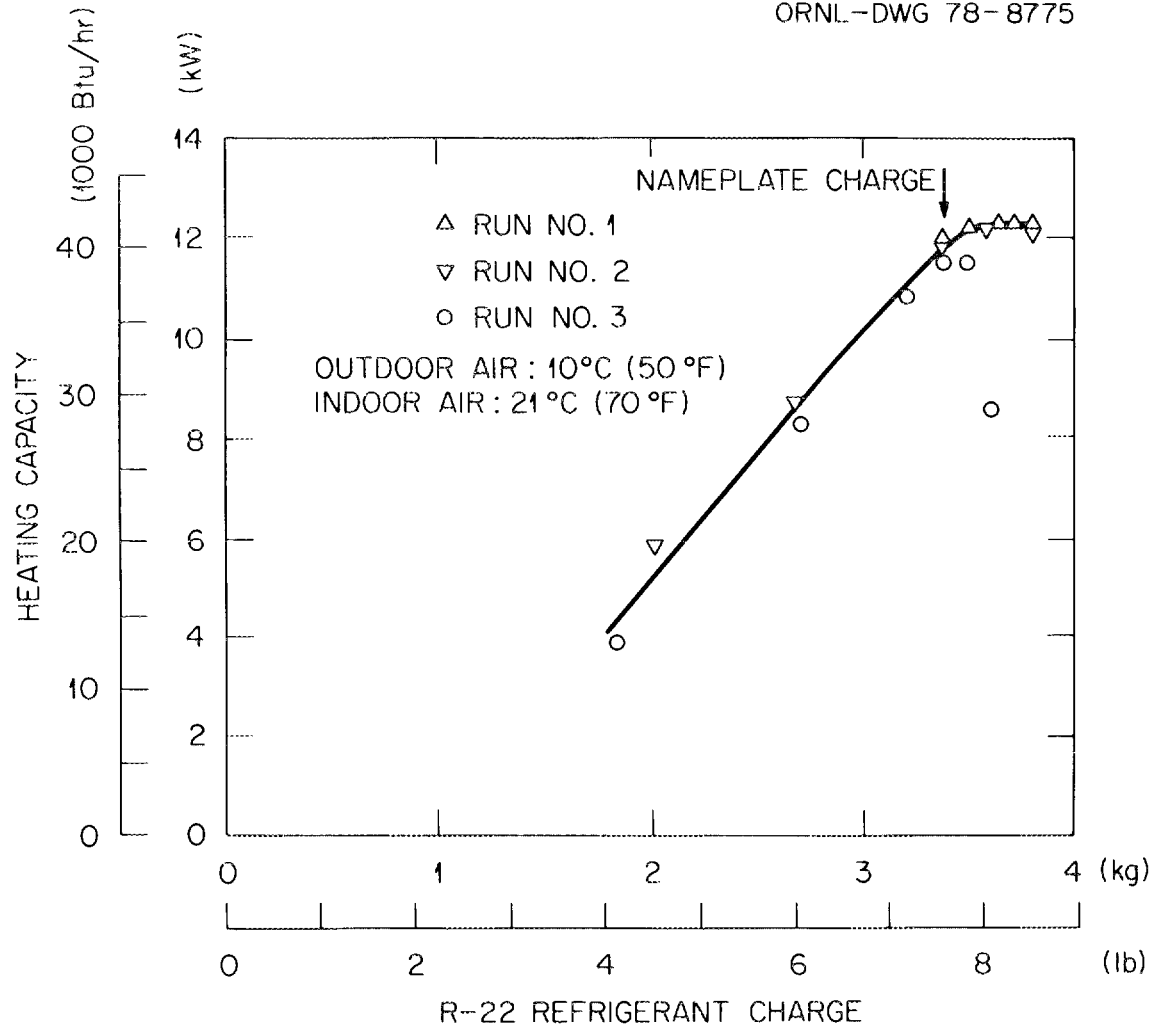


Fig. 8.4. Heating capacity as a function of refrigerant charge.

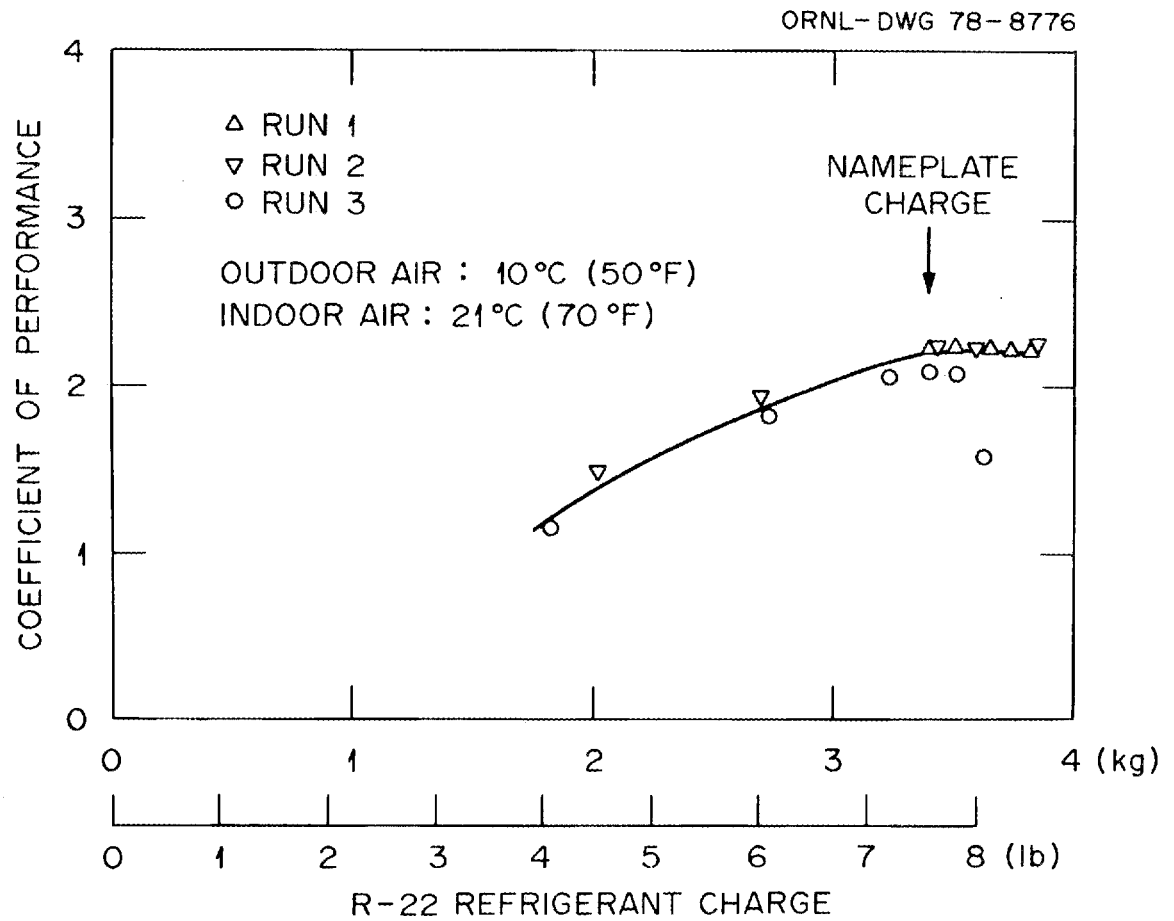


Fig. 8.5. COP as a function of refrigerant charge.

ACKNOWLEDGMENTS

The assistance of D. E. Holt, who was responsible for the assembly and operation of the laboratory apparatus, is gratefully acknowledged. S. J. Ball provided valuable advice in developing the computer program and data acquisition system. Sincere thanks is expressed to F. A. Creswick for his help in the evaluation of the experimental data and in the discussion of experimental procedures. J. E. Summers and N. E. Morgan helped solve instrument application problems. J. T. Farmer and C. R. Martin helped maintain the refrigerant loop in working condition.

REFERENCE

1. Federal Energy Administration, "Energy Conservation Program for Appliances," *Fed. Regist.* 42(155), 40828 (Aug. 11, 1977).

APPENDICES

Appendix A. SYSTEM DESCRIPTION

A.1. Heat-Pump Manufacturer Ratings and
Description of Heat-Pump Components

Refrigerant	R-22
<u>Heating capacity</u>	
At 8.3°C (47°F) outdoor air and 21°C (70°F) indoor air temperature	11.40 kW (39,000 Btu/hr)
At -8.3°C (17°F) outdoor air and 21°C (70°F) indoor air temperature	6.50 kW (22,000 Btu/hr)
<u>Coefficient of performance</u>	
At 8.3°C (47°F) outdoor air and 21°C (70°F) indoor air temperature	2.2
At -8.3°C (17°F) outdoor air and 21°C (70°F) indoor air temperature	1.4
<u>Cooling capacity</u>	
At 35°C (95°F) outdoor air temperature and 27°C (80°F) dry-bulb, 19°C (67°F) wet-bulb indoor air	10.55 kW (36,000 Btu/hr)
<u>Energy efficiency ratio</u>	6.3 Btu/hr·W
<u>Compressor</u>	
Type	Reciprocating, hermetic
Number of cylinders	2
Displacement	74.1 cm ³ (4.52 in. ³)
Speed (nominal)	3450 rpm
<u>Outdoor coil</u>	
Type	Copper tube and aluminum fins with return bends
Coil orientation	Horizontal
Fin thickness	0.16 mm (0.0063 in.)
Fin pitch	14 fins/in.
Tube outside diameter	9.5 mm (3/8 in.)
Face area	0.86 × 0.59 m (0.482 m ²) [34 × 22 in. (5.19 ft ²)]
Airflow, nominal	9000 m ³ /hr (2350 cfm)
Fan type	3 blades, propeller
Propeller diameter	0.51 m (20 in.)
Fan orientation	Horizontal axis
Fan location	Upstream of heat exchanger

Indoor coil

Type	Tube and fins with return bends
Orientation	Slanted
Fin thickness	0.16 m (0.0063 in.)
Fin pitch	14 fins/in.
Tube outside diameter	9.5 mm (3/8 in.)
Face area	0.48 × 0.56 m (0.269 m ²) [19 × 22 in. (2.9 ft ²)]
Airflow, nominal	2000 m ³ /hr (1200 cfm)
Fan type	Centrifugal, forward- curved impeller blades
Impeller diameter	0.23 m (9 in.) pitch diameter
Impeller length	0.20 m (8 in.)
Fan location	Downstream of heat exchanger

Refrigerant controls

Cooling	3 capillaries in parallel, 1.63 mm (0.064 in.) inside diameter, 0.76 m (30 in.) long
Heating	1 capillary, 2.03 mm (0.080 in.) inside diameter, 0.96 m (38 in.) long
Refrigerant reversing control	4-way valve
Charged tubing	
Length	7.62 m (25 ft)
Size	6.4 mm (0.25 in.) and 19.1 mm (0.75 in.)

A.2. Schematic and Details of the Outdoor and Indoor Heat Exchangers

A.2.1 Outdoor unit

Figure A.1 shows the inlet manifold on the outdoor coil and the four refrigerant streams originating at points 1, 2, 3, and 4. The refrigerant travels through the coils acting as evaporators in the heating mode and discharges as three streams into the collector before flowing downstream to the low side of the four-way refrigerant reversing valve. Figure A.2 displays the circuiting of the refrigerant return bends. The defrost sensor is located on one of the return bends at the bottom of the coil.

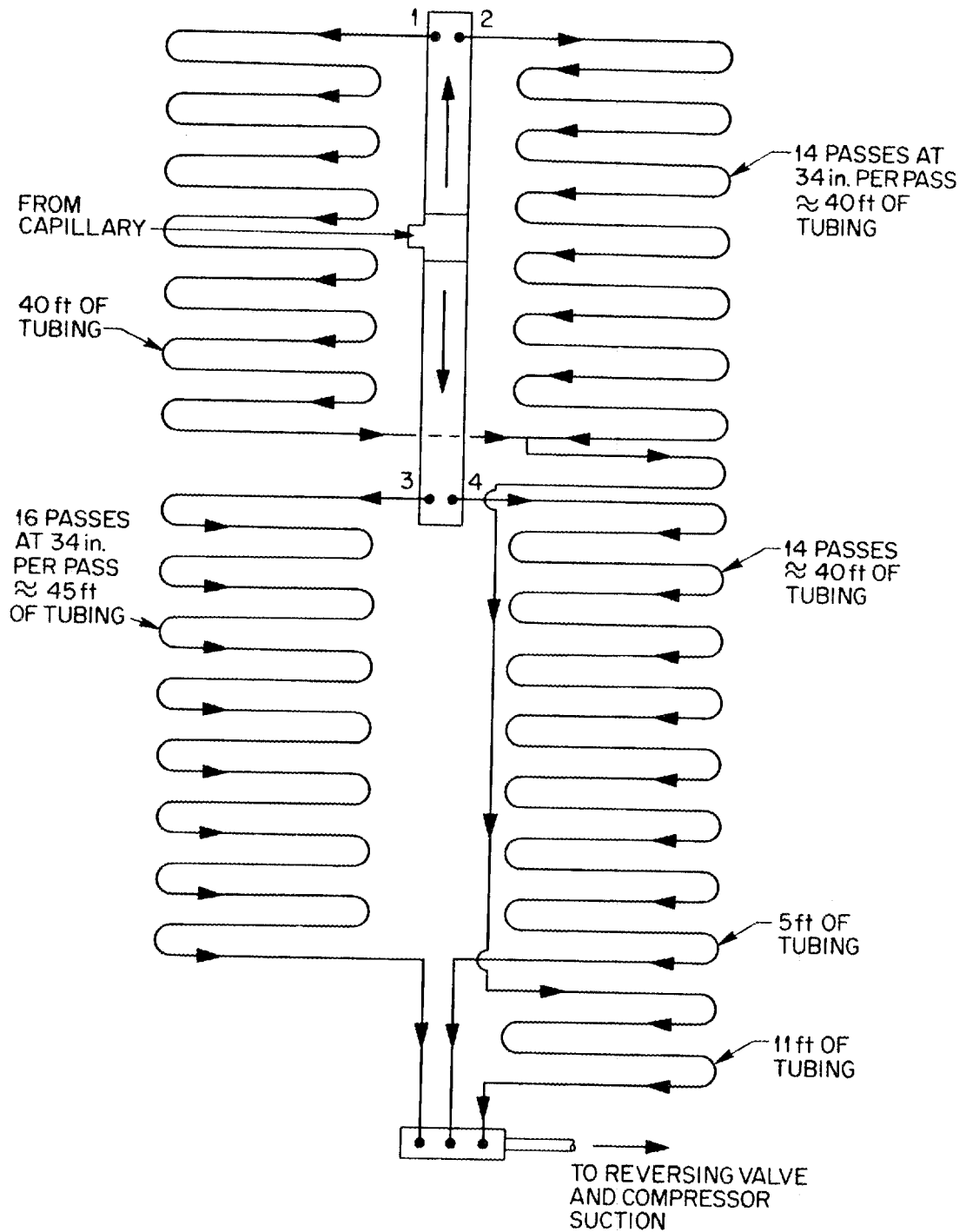


Fig. A.1. Schematic of outdoor-coil refrigerant circuit in the heating mode.

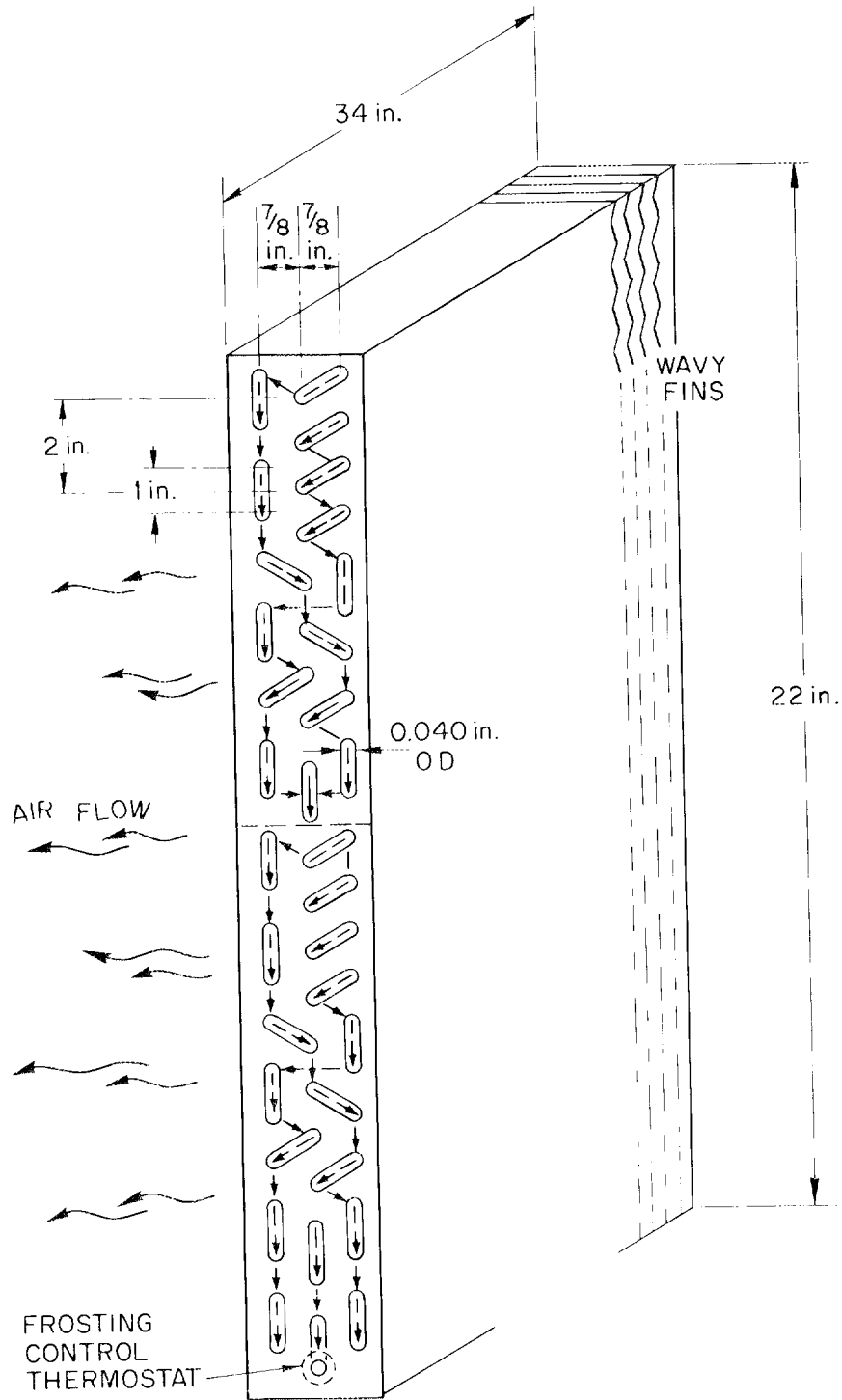


Fig. A.2. Outdoor-coil construction detail and refrigerant circuit in the heating mode.

A.2.2 Indoor unit

The relative positions of the centrifugal fan and the indoor heat exchanger are shown in Fig. A.3. The heat exchanger is inclined from the vertical. The fan, downstream from it, induces the air to the double-suction fan impeller. Figure A.4 shows the three parallel refrigerant circuits and the direction of the refrigerant flow in the heating mode.

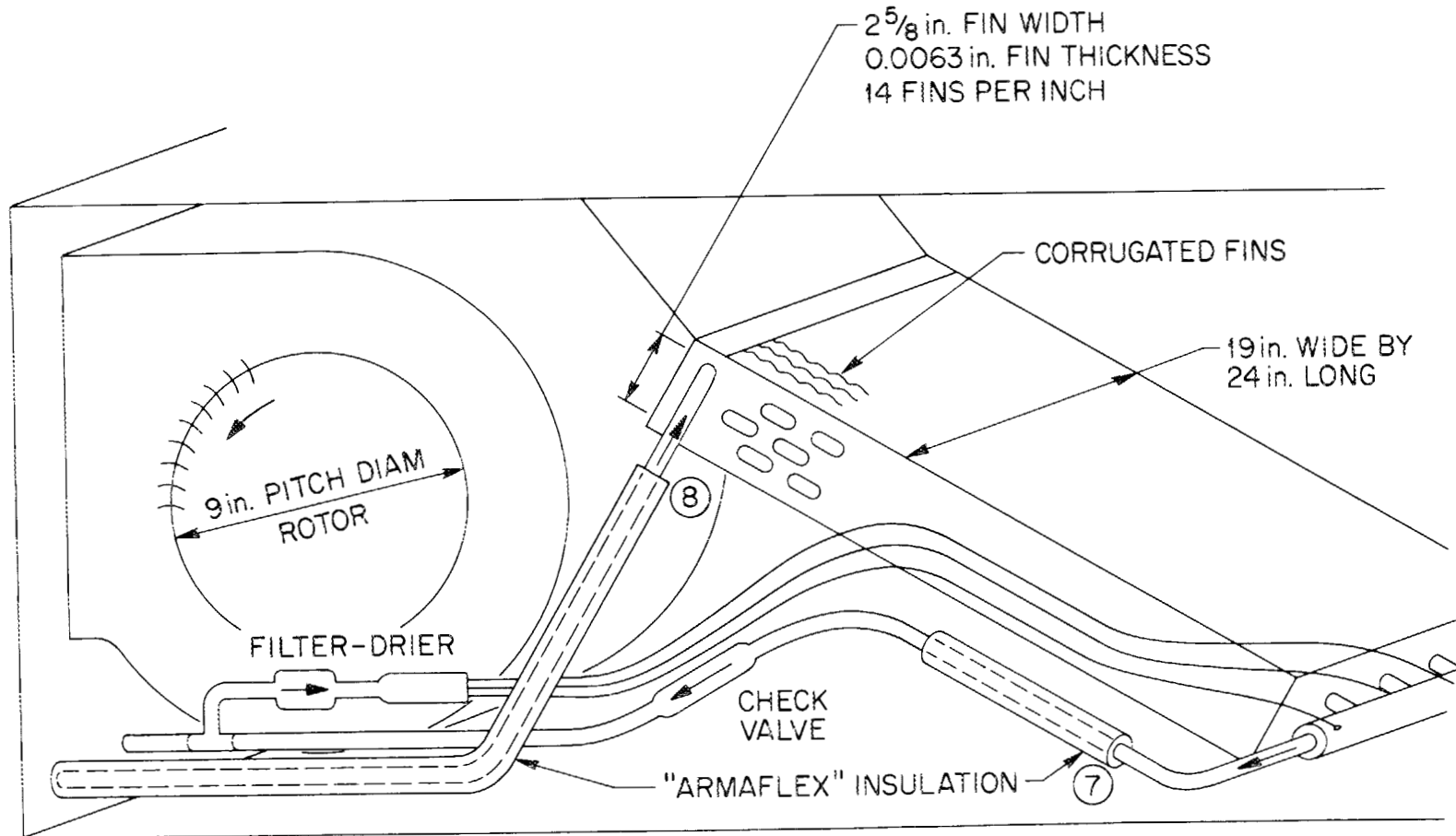


Fig. A.3. Indoor unit schematic.

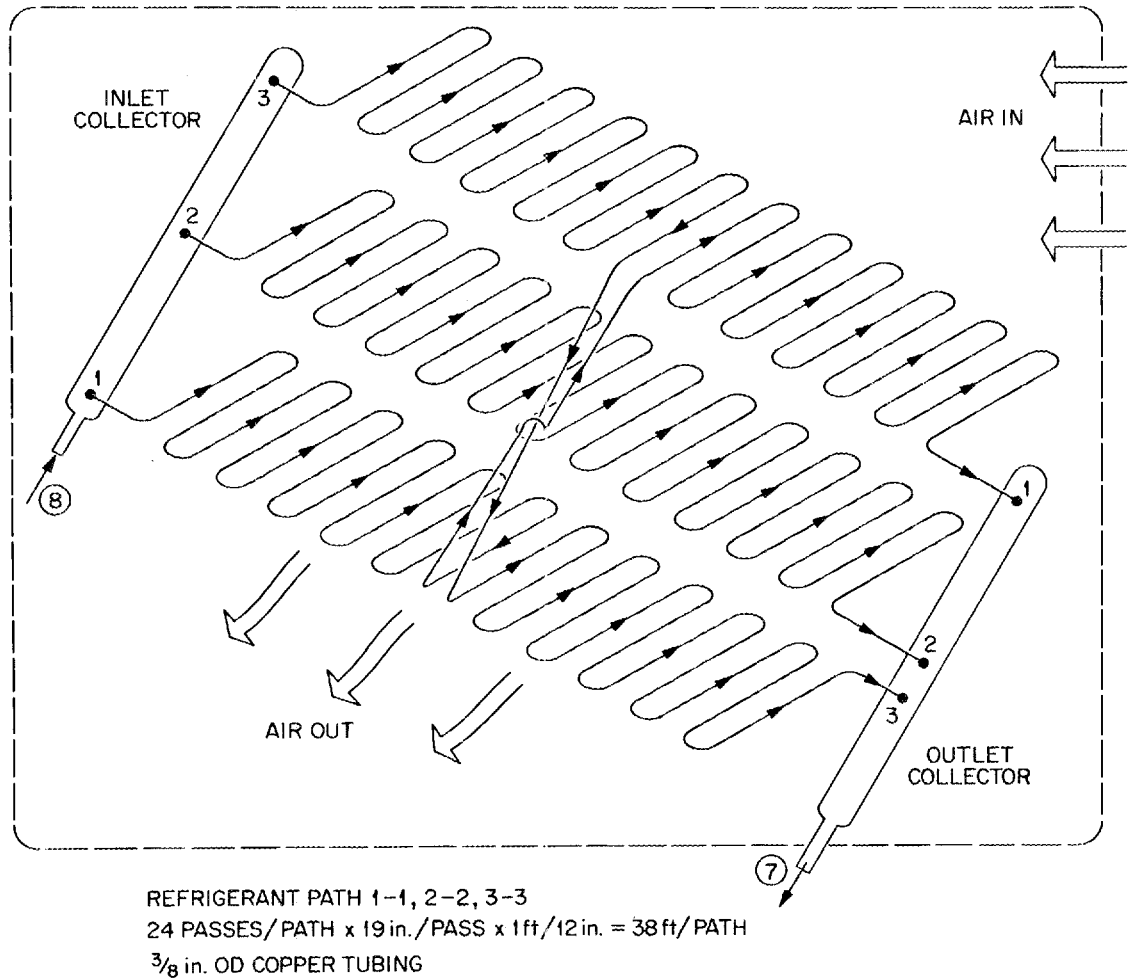


Fig. A.4. Schematic of indoor-coil refrigerant circuit in the heating mode.

Appendix B. STEADY-STATE (NO-FROST) EXPERIMENTAL DATA

Table B.1 shows the data collected and the results of some of the computations needed for evaluating the performance of the heat-pump system operating under no-frost conditions in the heating mode. Figure B.1 shows the location of the heat-pump components and the refrigerant flow path in the heating mode. Included in the figure is the pressure-enthalpy diagram for R-22. The numbered points on the diagram correspond to numbered points on the circuit diagram.

Table B.1. Steady-state test data

Run No.	Date	Air temperatures, °F				Refrigerant temperatures, °F							Pressures, psia			Airflow rate, cfm		Airflow rate, indoor coil, lb/hr	Refrig. flow rate, lb/hr	Power input, W		Power input, kW		Heating capacity, kW		COP			
		Outdoor coil		Indoor coil		Evap. in	Evap. out	Comp. in	Comp. out	Rev. valve out	Cond. in	Cond. out	Cap. tube in	Atmos. press., in. Hg	Comp. suct.	Cap. tube in	Comp. disch. (est.)			Out-door coil	In-door coil	Outdoor fan	Indoor fan	Compressor	Total	Refrig. method	Air method	Refrig. method	Air method
		In	Out	In	Out																								
1	12/14/76	64.3	52.5	72.6	107.6	48.4	63.1	67.2	251	234.3	223.8	81.8	80.1	29.2	76	325	335	2330	1230	5320	383	458	587	4.66	5.71	12.15	13.10	2.13	2.29
2	12/15/76	51.0	41.5	69.6	101.5	42.4	49.5	53.7	229	213.2	205.5	77.7	75.9	29.3	67.5	295	305	2160	1210	5350	353	499	590	4.17	5.28	10.88	11.99	2.06	2.27
3	12/15/76	26.5	21.9	71.7	96.2	25.7	20.1	15.7	178	158.9	160.4	78.0	72.5	29.3	53.5	250	260	2150	1220	5300	295	519	593	3.67	4.78	8.64	9.14	1.81	1.91
4	12/17/76	41.2	33.6	71.4	105.3	37.9	32.1	28.9	217	198.8	196.3	82.0	78.2	29.3	66.2	297	307	2200	1080	4690	352	501	469	4.19	5.16	10.46	11.17	2.03	2.16
5	12/17/76	51.7	42.1	71.4	109.4	44.8	48.3	52.2	237	221.8	216.1	83.9	81.0	29.3	73	322	332	2110	1080	4690	374	484	469	4.56	5.51	11.14	12.52	2.02	2.03
6	12/20/76	29.6	25.2	72.4	101.3	29.4	22.3	19.0	180	162.2	165.1	82.0	76.2	29.3	57	270	280	2160	1080	4620	319	515	469	3.84	4.82	8.92	9.39	1.85	1.95
7	1/12/77	26.7	22.3	71.1	103.6	27.0	20.0	16.3	167	147.0	155.0	85.7	78.8	28.9	55	275	285	2260	790	3400	310	516	390	3.91	4.82	8.92	7.77	1.74	1.61
8	1/12/77	44.2	35.8	71.1	113.9	41.0	34.1	29.2	222	202.3	204.5	90.1	85.3	28.9	70	320	330	2170	780	3350	363	506	384	4.54	5.32	10.39	10.09	1.91	1.85
9	1/12/77	33.9	27.5	70.3	106.8	33.2	25.5	21.2	188	167.9	172.9	86.2	79.9	28.9	60	290	300	2230	750	3220	328	511	388	4.01	4.91	9.04	8.25	1.84	1.68
10	1/17/77	41.7	33.5	72.5	101.2	37.6	38.7	42.8	224	206.6	201.7	71.0	75.7	28.9	63	275	285	2300	1230	5280	329	511	608	4.09	5.21	10.59	10.69	2.03	2.05
11	1/18/77	53.8	45.1	65.4	97.9	43.4	54.1	58.9	237	220.0	210.8	73.1	71.8	29.0	66	245	255	2240	1150	5000	329	498	579	4.14	5.22	10.56	11.41	2.02	2.19
12	1/17/77	42.0	34.1	65.3	94.8	36.0	40.5	45.1	221	203.9	196.8	72.3	69.0	28.9	61	260	270	2310	1110	4830	320	514	603	3.88	5.00	10.21	10.02	2.04	2.00
13	1/17/77	31.3	24.8	65.6	92.0	29.2	22.3	19.3	202	181.3	178.3	71.9	67.6	28.9	55	238	248	2240	1100	4810	292	519	612	3.61	4.74	9.00	8.90	1.90	1.87
14	1/18/77	31.1	25.4	81.0	105.9	30.6	23.1	19.0	189	168.2	172.1	88.8	82.1	29.0	57	278	288	2440	1150	4850	307	511	587	3.85	4.95	8.68	8.45	1.75	1.72
15	1/18/77	49.6	40.5	82.6	114.2	44.3	46.0	50.5	244	226.1	223.0	92.1	87.9	29.0	71	327	337	2370	1130	4720	359	498	585	4.80	5.88	10.41	10.48	1.77	1.78
16	1/18/77	42.4	34.2	80.4	110.0	39.2	34.9	38.8	226	209.0	207.4	89.5	84.1	29.0	66	310	320	2390	1140	4790	338	505	587	4.26	5.35	10.19	10.63	1.90	1.99
17	2/2/77	12.0	9.7	71.6	90.2	14.2	7.9	5.0	135	114.5	125.0	77.1	67.8	29.5	43	211	221	2370	1200	5230	223	535	608	3.52	4.66	6.33	6.82	1.35	1.46
18	2/2/77	26.9	20.7	70.5	93.8	25.8	18.9	14.0	185	164.8	166.7	76.4	70.3	29.5	52	240	250	2370	1170	5130	283	535	609	3.60	4.74	8.63	8.41	1.82	1.77
19	2/2/77	37.5	30.1	72.5	100.0	34.4	33.3	37.2	218	202.4	201.2	79.4	75.1	29.5	60	265	275	2210	1100	4750	312	499	590	3.96	5.05	9.87	9.23	1.96	1.83

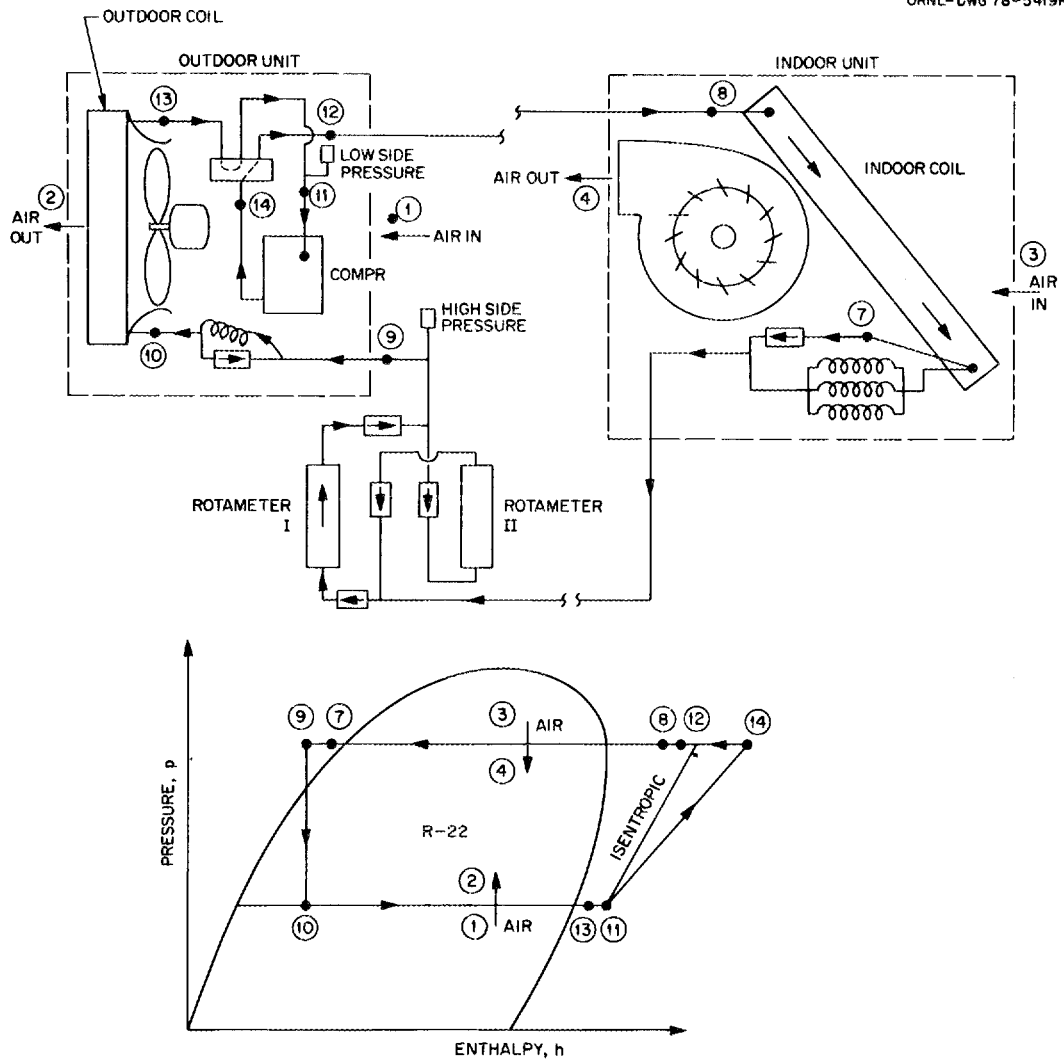


Fig. B.1. Schematic of refrigerant circuit, air path, and thermodynamic cycle in the heating mode.

Appendix C. FAN-MOTOR PERFORMANCE CURVES

C.1. Centrifugal Fan (Indoor Unit)

Table C.1 incorporates the three runs utilized to determine the head-capacity and power-capacity curves for the indoor fan.

Table C.1. Indoor-fan test data

Run No.	Volume rate of air (cfm)	Static-developed head, Δp_s (in. H ₂ O)	Fan-motor input power (kW)
1	1190	0.76	0.621
2	1183	0.82	0.600
3	1038	0.96	0.541

The information contained in Table C.1 was used to compute the overall efficiency of the fan-motor unit for a volumetric airflow rate between 1000 and 1250 cfm. This is shown in metric and English units in Table C.2.

Table C.2. Overall efficiency of the indoor-fan-motor unit as a function of airflow rate

Volumetric flow rate [m ³ /hr (cfm)]	Static-developed head [kPa (in. H ₂ O)]	Air power (kW)	Power input (kW)	Overall efficiency
1670 (1000)	0.24 (0.98)	0.113	0.522	0.216
1870 (1100)	0.22 (0.90)	0.114	0.571	0.200
1950 (1150)	0.21 (0.84)	0.111	0.598	0.186
2040 (1200)	0.19 (0.75)	0.103	0.621	0.166
2120 (1250)	0.16 (0.66)	0.095	0.645	0.147

C.2. Propeller Fan (Outdoor Unit)

The three experimental runs used to obtain the head-capacity and input-power-capacity curves for the outdoor fan are displayed in Table C.3.

Table C.3. Outdoor-fan test data

Run No.	Volumetric flow rate (cfm)	Static-developed head, Δp_s (in. H ₂ O)	Fan-motor input power (kW)
1	2075	0.26	0.488
2	1510	0.35	0.510
3	1880	0.30	0.498

The overall fan efficiency as a function of the volumetric airflow rate is displayed in Table C.4. Values were obtained from extrapolation and interpolation of the data in Table C.3.

Table C.4. Overall efficiency of the outdoor-fan-motor unit as a function of airflow rate

Volumetric airflow rate [m ³ /hr (cfm)]	Static-developed head [kPa (in. H ₂ O)]	Air power (kW)	Power input (kW)	Overall efficiency
2550 (1500)	0.087 (0.35)	0.060	0.510	0.118
2890 (1700)	0.082 (0.33)	0.064	0.504	0.128
3230 (1900)	0.073 (0.295)	0.064	0.498	0.129
3400 (2000)	0.068 (0.275)	0.063	0.494	0.128
3570 (2100)	0.062 (0.25)	0.060	0.489	0.123
3740 (2200)	0.057 (0.23)	0.058	0.481	0.121
3910 (2300)	0.051 (0.205)	0.054	0.475	0.114

INTERNAL DISTRIBUTION

ORNL/CON-18

- | | |
|-----------------------|-----------------------------------|
| 1. S. I. Auerbach | 32. H. M. Long |
| 2. M. Baker | 33-52. P. M. Love |
| 3. S. J. Ball | 53. R. N. Lyon |
| 4. V. D. Baxter | 54. C. R. Martin |
| 5. S. E. Beall | 55. J. W. Michel |
| 6. D. J. Bjornstad | 56-75. R. E. Minturn |
| 7. J. R. Buchanan | 76. W. R. Mixon |
| 8. R. S. Carlsmith | 77. N. E. Morgan |
| 9. W. S. Chern | 78. J. C. Moyers |
| 10. C. V. Chester | 79. E. A. Nephew |
| 11. T. J. Clifford | 80. D. L. O'Neal |
| 12. F. A. Creswick | 81. H. Postma |
| 13. R. M. Davis | 82. M. W. Rosenthal |
| 14. J. G. Delene | 83. T. H. Row |
| 15. A. A. Domingorena | 84. G. G. Slaughter |
| 16. R. D. Ellison | 85. R. L. Spore |
| 17. J. T. Farmer | 86. E. G. Struxness |
| 18. W. Fulkerson | 87. J. E. Summers |
| 19. V. O. Haynes | 88. D. B. Trauger |
| 20. N. E. Hinkle | 89. G. U. Ulrikson |
| 21. E. A. Hirst | 90. D. J. Walukas |
| 22. E. C. Hise | 91. T. J. Wilbanks |
| 23. A. S. Holman | 92. J. V. Wilson |
| 24. D. E. Holt | 93. H. E. Zittel |
| 25. C. C. Hopkins | 94. A. Zucker |
| 26. J. R. Jackson | 95. Biology Division Library |
| 27. W. L. Jackson | 96-97. Central Research Library |
| 28. P. L. Johnson | 98. Document Reference Section |
| 29. S. I. Kaplan | 99. Laboratory Records - RC |
| 30. D. Kaserman | 100-102. Laboratory Records Dept. |
| 31. R. S. Livingston | 103. ORNL Patent Office |

EXTERNAL DISTRIBUTION

104. Mr. Roy Abbott, Advance Technology Operations, General Electric Company, AP6, Appliance Park, Louisville, KY 40225
105. Dr. Ervin Bales, Department of Energy, Division of Buildings and Community Systems, 20 Massachusetts Avenue NW, Washington, D.C. 20545
106. Mr. Robert Boyd, National Association of Home Builders, Post Office Box 1627, 627 Southlawn Lane, Rockville, MD 20850
107. Mr. B. Cleveland, DuraTherm Company, LaGrange, Indiana 46761
108. Mr. E. G. Ehlers, Electric Power Research Institute, Palo Alto, CA 94304
109. Mr. G. W. Gatecliff, Research Laboratory, Tecumseh Products Company, Ann Arbor, MI 48105

110. Dr. L. R. Glicksman, Department of Mechanical Engineering, Massachusetts Institute of Technology, Cambridge, MA 02139
111. Mr. S. D. Goldstein, Advanced Energy Systems, Exxon Enterprises, Inc., Post Office Box 192, Florham Park, NJ 07932
112. Mr. Gerald C. Groff, Research Division, Carrier Corporation, Syracuse, NY 13201
113. Dr. C. C. Hiller, Sandia Laboratories, Livermore, CA 94550
114. Mr. F. Honnold, Consumer Products Division, Carrier Corporation, Syracuse, NY 13201
115. Mr. T. Jacoby, Tecumseh Products Company, Tecumseh, MI 49286
116. Mr. H. Jaster, General Electric Corporate Research and Development, General Electric Company, Schenectady, NY 12301
117. Mr. Ralph Johnson, National Association of Home Builders, Post Office Box 1627, 627 Southlawn Lane, Rockville, MD 20850
118. Mr. F. Kalivoda, Copeland Corporation, Sydney, OH 45365
119. Mr. Rube Kelto, Tecumseh Products Company, Tecumseh, MI 49286
120. Mr. R. W. King, Copeland Corporation, Sydney, OH 45365
121. Mr. L. L. Lawrence, Gas Research Institute, Chicago, IL 60690
122. Mr. N. Nenov, Linde Division, Union Carbide Corporation, Tonawanda, NY 14150
123. Mr. Michael Perlsweig, Department of Energy, Division of Conservation Research and Technology, 20 Massachusetts Avenue NW, Washington, D.C. 20545
124. Mr. J. A. Pietsch, General Electric Company, Troup Highway, Tyler, TX 75711
125. Mr. P. J. Reynolds, Department of Energy, Division of Buildings and Community Systems, 20 Massachusetts Avenue NW, Washington, D.C. 20545
126. Mr. D. E. Scherpereel, Research and Engineering Center, Whirlpool Corporation, Benton Harbor, MI 49022
127. Dr. M. H. Somerville, Engineering Experiment Station, University of North Dakota, Grand Forks, ND 58202
128. Mr. W. F. Stoecker, University of Illinois, Urbana, IL 61801
129. Mr. M. Wilden, University of New Mexico, Albuquerque, NM 87115
130. Institute of Energy Analysis, ORAU Library
131. Research and Technical Support Division, DOE-ORO
- 132--158. Technical Information Center, DOE, Post Office Box 62, Oak Ridge, TN 37830
- 159--600. External Energy Conservation Distribution Mailing List and Energy Conservation Office (9102-1, Room 2).